Towards active matter on deformable surfaces

An Honors Thesis for the Department of Physics and Astronomy

Ian Hunter under advisor Professor Tim. Atherton

Abstract:

This thesis is the result of trying to computationally model the fascinating dynamics which have been experimentally observed to arise between deformable surfaces and active matter in a generalized framework which future researchers can use. Consequently this thesis is concerned with analyzing the prospect of using the programming language Morpho as a platform for this purpose. In doing so Morpho's ability to model liquid, soft solid interfaces, and active matter on surfaces will be analyzed. Further analysis of a model of polar active matter confined to a hard sphere will serve as an example of how the organization of active matter on surfaces develops.

Acknowledgements:

The pursuit of this project was only possible through the guidance of Professor Tim Atherton and Andrew DeBenedictis. Professor Tim Atherton suggested this fascinating topic, and taught me much of the background necessary to pursue it. Further without the programming language Morpho, which he wrote, this project would have been impossible. Since spending a summer working with him as an official graduate mentor, Andrew DeBenedictis has provided excellent advice on how I should conduct my research on a day-to-day basis and helped me understand the advanced mathematics at work in this problem. Further I am thankful for Professor Peter Love for taking the time to give his expert feedback on my work by serving as a thesis reader alongside Professor Atherton. Also I am indebted to Chris Burke, Andrew Mascioli, and Matt Peterson for their willingness to discuss physics and computation. Similarly I owe much to Matt DiRe's willingness to discuss topology with me.

Contents

Introduction:

Even as physics is now beginning to describe the outer reaches of our universe and which fundamental particles compose all matter, it has only recently begun to be used to explore the mechanics of living beings and groups of them. Though biology has explored these dynamics, it has rarely been able to construct mathematical models of them that can predict either how similar systems behave, or how to assemble systems which function similarly. Physicists in the active and soft matter fields have begun to create precise models of how microscopic and macroscopic biological systems function. Two of many recent advances in the active and soft matter fields are the successful mathematical modeling of bacteria flow, and the mechanical properties of our tissues such as veins in differing chemical environments [34, 19].

Two universal components to cellular biology are soft membranes, and components which turn nutrients into motion. Active matter, matter which turns supplied energy into correlated motion, has been thoroughly mathematically described when submerged in liquid or fixed to an immobile surface. Analysis of the interplay between liquids, soft membranous surfaces, and active matter has been pursued. Yet a larger theoretical framework which allows one to predict the behavior of a variety of active matter systems on arbitrary deformable surfaces is yet to be created.

In chapter 1 the phenomena of deformability, progress in modeling it, and comparison to relevant experiments will be explored. This will include a discussion of two distinct classes of deformable surfaces, soft solids and liquids. Past models of deformability will be discussed, as will the technique used by Morpho called gradient descent. The success of Morpho in replicating the behavior of both stationary and dynamic soft solid and liquid experimentally observed behavior will be tested.

The second chapter will focus on active matter. Analytical and numerical investigations of the behavior of active matter in liquids, on hard surfaces, and within elastic bulks will be detailed. Past and original work respectively analyzing the phase transitions exhibited by polar active matter on hard toroids, and spheres will be explored.

The final chapter details experiments which show the rich behavior of active matter systems on deformable surfaces and potential ways of combining active matter, and deformable surfaces in Morpho. A full comparison between an active matter system on a deformable surface, and experimental results did not prove feasible during the course of research. During this time key potential issues related modeling the motion of active particles along the representations of surfaces Morpho uses were discovered. Advice for future researchers on how to sidestep these pitfalls will be articulated.

Chapter 1

Deformable Surfaces:

Deformable surfaces are common and intuitive to explain. A deformable surface is a surface, which when subject to an applied force or due to internal forces, can form another surface. In fact all surfaces are deformable by this definition, however for almost all purposes there are many surfaces, such as brick walls, which are not deformable; the forces in systems containing brick walls are generally incapable of changing them.

In spite of their omnipresence and apparent simplicity, deformable surfaces are difficult to describe. Firstly a surface represents a continuous and connected region. Deformable surfaces are composed of vast collections of particles whose collective collisions and interactions determine the change in the surface's shape. Trying to solve a system of equations of the equations of motions for each of the many billions of particles in these systems will not be fruitful. Secondly, since we have abandoned the notion that we can describe deformable surfaces through simply understanding their molecular composition, it is not immediately clear how to differentiate between the different types of deformable surfaces. For example polymer-air interface and rubber-air interface are both deformable surfaces, yet they have been observed to behave differently [15].

This situation is further complicated if we are concerned with the dynamic evolution of deformable surfaces, not just the static equilibrium configurations of a surface.

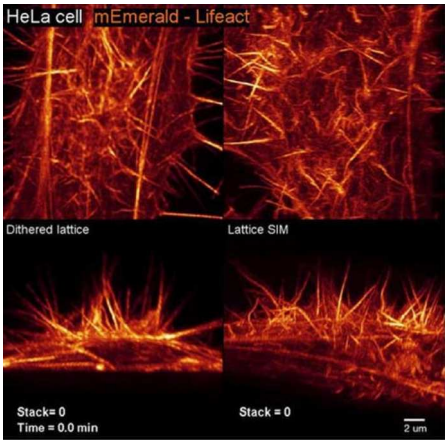

Figure 1.0.1: HeLa cell undergoing filopodia [7]

The space of possible deformable surface dynamics subject to discussion in this thesis, is confined to the still expansive domain of deformable surfaces which can be appreciably altered by active matter traveling along their surfaces. Deformable surfaces, such as a block of rubber, can be quite tough to deform. The motions of microscopic active matter components cannot easily alter the surface of a solid piece of rubber, and as a result there is a dearth of experimental investigations of their coupled dynamics. Instead deformable surfaces which are composed of liquids, or flowing soft solids such as lipids will be the subject of investigation. Modeling this domain would include a wide range of biological systems in which cells are predominantly composed of lipids. Also within this domain there exist established experimental, and well-grounded analytical results to compare to [17, 16]. Further this thesis seeks to model accurately the features which appear on liquid and soft solid surfaces. The motivation for this being that recent high resolution pictures of cells reveal that they are not round, but instead covered in peaked features

fig:1.0.1. It has been experimentally proven that active matter traversing lipid vesicles can produce these cilia-like features [17]. For this reason, despite the fact many models ignore surface features, the ability to model surfaces features will be considered one of the chief measures of success of this model.

Throughout the following chapter a distinction will be made between soft solid and liquid surfaces due to the impression that they concisely describe two classes of deformable surfaces which experimentally exhibit distinct behavior. Interfaces composed of constituents which flow only in response to external stimuli, and their own momentum will be labeled as liquids. Traditionally these have been labeled as viscous liquids. On the other hand interfaces of molecules which flow additionally in response to the elasticity of the molecules will be known as soft solids. These are also known as viscoelastic liquids. As will be shown in the following sections on relevant experimental work 1.2.3 1.2.4, liquids and soft solids exhibit different static and dynamic behavior.

1.1 Established modeling techniques:

1.1.1 Liquid modeling:

Due to the fact oil tanker ships, and spacecraft all contain large amounts of liquid, the drive to understand how to suppress energetic perturbations of vehicle movement by the liquids they contain has been thorough investigated. The dynamics of confined liquids, known as sloshing, were first described in the 1960s in rectangular and cylindrical containers via a Kelvin's equation for unsteady fluid flow with gravity. Provided the liquid was incompressible and stationary, this equation becomes Laplace's equation [14]. This is problematic for our purposes, as is shown during the derivation of area minimal solutions 4.1, Laplace's equations are a linearization of liquid dynamics which fail to

capture highly curved surface features. Generally since then however it is noted that scientists have chosen to model liquids through minimizing a Lagrangian formulation of the liquid's surface. For liquids in containers the Euler-Lagrange equation minimized is proportional to the velocity potential squared, which is determined by the liquid and the motion of the container, and the surface energy of the liquid's surface[14].

The study of liquids interacting with a solid surface, wetting, has described a wide range of static equilibrium behavior as an energy minimization problem. Young and Wenzel equations and Cassie–Baxter equations were created at first phenomenologically to predict the measured angle between the tangent along the liquid-gas interface and perpendicular the surface on smooth and rough surfaces. Though these equations assume the drop is on a perfectly smooth solid surface, and experimentally line tension prevents complete relaxation to this value, the variations in contact angle are closely about the values they predict [4, 28]. These equations can be derived from allowing the radius and profile of the droplet to change in order to minimize the energy of surface tensions between the drop, gas, and solid interfaces [5].

It might seem natural that our approach to modeling liquids follow from oceanic modeling, exclusively focused on modeling water, however said methods are dedicated to solving either non-linear behavior along shorelines, or that of slow motion of massive volumes of water. Oceanography is currently able to predict global tides years in advance through solving Laplace's tidal equations given approximate knowledge of the ocean floor, coastlines, and motion of the moon [23]. As aforementioned Laplace's equations fail to capture curved features which, unnecessary for calculating global currents, are essential for modeling biological systems. The modeling of shorelines is taken as an extreme type of sloshing in which high magnitude external forces water periodically

onto a hard surface. As a result of the external forcing being much larger than that found unavoidably in human containers of liquids, the non-linear phenomena of cresting and falling of waves is an essential component of shoreline modeling. Consequently these models, most commonly Cubic Interpolated Psuedo Particle models, must allow liquids to form psuedo particles which can be ejected from the bulk and recombine [12]. As cresting waves are not found in biological systems the heavy computational cost of simulating this transition is not worthwhile.

1.1.2 Soft solid modeling:

Generally modeling the deformation of soft solids is treated analytically based upon minimizing the energy of the bulk in question. Rather than using thermodynamic, or molecular evolution equations for the many particles of the system, direct minimization of the phenomenological quantities associated with the energy of the media, called the Onsager principle, is seen as the most expedient approach [9]. This is due to the fact that when concerned with systems which are far out of equilibrium, and composed of particles whose motion are potentially correlated through non-local interactions, many thermodynamic equations become inaccurate. An example of the analytical use of this approach is that for a sheet of material of surface area S, and height h between parallel plates, whose energy, $U(x)$, and damping, ζ_{ij}, is described in a Rayleighian equation of the form $R = \sum_j \zeta_{ij}(x)\dot{x}_j - \frac{\partial U(x)}{\partial x_i}$. About equilibrium the shear stress, a commonly measurable quantity of materials, is $\sigma_{xy}(t) = \frac{1}{Sh}\frac{\partial R}{\partial \dot{\gamma}}$ [9]. While in systems where U depends on only 1 variable this approach seems incredibly simple, soft solids of interests typically are modeled correctly only through minimization of more intricate potentials.

Using the Onsager principle the motion of self-organizing surfaces composed

of anisotropic surfactant molecules can be posed simply, though rarely solved analytically. Since such surfaces have energies associated with their curvature, to quadratic order their energies must be equal to:

$$\int_S 2\kappa(H - C_o)^2 + \kappa_G K_G dS$$

where H, C_o, and K_G are the surface's mean, spontaneous, and Gaussian curvature[29]. Ignoring additional curvature terms which depend on particle density, and imposing constraints on the area and volume of the surface yields the total energy equation to be minimized[29, 21]:

$$\int_S \sigma + 2\kappa(H - C_o)^2 + \kappa_G K_G dS - \int_V P dV$$

As by the Gauss-Bonnet theorem over any manifold M $\int_M K_G dS = 2\pi\chi(M)$, where $\chi(M)$ is the Euler Characteristic of the surface which is invariant under distortions and thus cannot be minimized, the third term is ignored.

Two examples of previous soft solid computational models based upon the Onsager principle include models of minute deformations to a vesicle, and smooth deformations of whole vesicles. The first model, which due to its consideration of point-like deformations, is posed as solving for the minimal curvature energy between a raised inner radius and a larger outer radius representing the outer extent of the deformation, and the nearby attached bulk of the vesicle. For the sake of tractability spontaneous curvature was set to 0, a poor assumption for the modeling of lipids [9], and volume conservation was considered negligible. Thus the total energy was $\int_S \sigma + \frac{2\kappa}{\mu} H^2 dS$. The Euler-Lagrange formulation of this total energy was then minimized using gradient descent. When the H term was eliminated, the resulting structures were catenoids connecting the raised inner radius to the outer radius. Minimization

of the full expression led to the stabilization of fine inner radii deflections raised to heights comparable to the scale of the outer radius in a structure which resembles a smoothly capped cylinder emerging from the bulk with a catenoidal connecting region [24]. Another model also uses the Onsager principle to calculate the equilibrium states of cells whose curvature gives them smooth non-spherical shapes such as red blood cells. As a result it approximates the surfaces with spherical harmonics over fewer than 400 grid points. The spherical harmonics are moved via conjugate gradient descent to minimize the full density independent curvature energy functional $\int_S \sigma + 2\kappa(H - C_o)^2 + \kappa_G K_G dS$, with surface area and volume constraints elastically enforced. While this method was able to closely approximate the shapes of red blood cells with certain numbers of spherical harmonics, too few or too many provided poor approximations[21]. The inability of this model to capture peaked surface features makes it uninteresting for the purpose of modeling active matter deformable surface coupling. It does however provide evidence of the robustness of the energy minimization approach to modeling soft solids. Elastically enforcing constraints rather than directly preventing energy minimization methods from violating constraints may have a place in modeling of biological systems as it allows systems to be disrupted from equilibrium. See appendix entry 4.2 for an example of how enforcing a direct linearization of constraints on a system being taken out of equilibrium can result in unphysical behavior.

Coarse-grained simulations have provided a means of exploring the metastable configuration of vesicles composed of nematic liquid crystals such as lipids. Motivated by describing the irregular metastable configurations that large lipid vesicles form when in solution and thus externally unimpeded from reaching the surface energy minimal spherical configuration. [13]. In polydisperse lipid vesicles the different types of lipids separate into domains of like lipids,

causing curvature irregularity along the vesicle surface. Monodisperse lipid vesicles, when cooled, or placed in ionic solutions, from a surface minimal spherical configuration will become exceedingly deformed[13]. Models of lipid vesicle irregularity have, instead of minimizing a particular energy, numerically integrated clumps of vesicle idealized as points with complex localized potentials about them. These potentials have been constructed based upon how the species of vesicle forming nematic interact, with one another, and the solvent that implicitly surrounds them qualitatively [35] or mathematically [11]. These models have been able to replicate both of the features of interest about lipids, and allow the particles to freely form the vesicle phase or explore others. Though they hold insight in the case in which one is curious about phase diagrams of nematic liquid crystals in a solution, the freedom of particles to disassociate with the surface would make moving active particles across the surfaces formed in these models unnecessarily difficult. Never the less any model of vesicle deformation must be able to replicate the same results.

1.2 Computational deformation modeling:

1.2.1 Deformation as an energy minimization problem:

Though energy minimal models of deformable surfaces idealize the energy in the system they seek to model, and are thus at times labeled phenomenological, they are physically well motivated. Modeling a surface in terms of minimizing curvature and area energies ignores the dynamics of the molecules in the bulk of the surface. This has led many authors and publishers to refer to these models as phenomenological, implicitly as opposed to simulations which directly simulate the constituents of the surface and bulk. Yet Hamiltonian and Euler-Lagrange formalism are used without a second thought when describing

pendulums, balls, and other macroscopic systems; ignoring the details of the individual molecules composing these systems instead focusing on minimization of macroscopic energies. Thus energy minimization models of surfaces are no more phenomenological than the equations which are used to describe all manner of physical systems. Similar to springs with well-defined elastic constants, surfaces composed of vast numbers of constituents have well-defined surface curvatures which can be measured. Any given energy minimization parametrization of the surface in terms of these curvatures might not model the surface. However the surface and thus its curvatures must be conserving energy in some respect to guarantee time invariance as its curvature continues to be well-defined and measurable.

Acknowledging the past success of energy minimization models of surfaces, and the solid theoretical footing of the technique, it was chosen as the method for modeling deformable surfaces during this project. The past success of energy minimization techniques served as a powerful motivation for its selection. Further the fact that energy minimization of curvature energies can be generalized to arbitrary surfaces made it an excellent choice. As a result this technique could be used to create a program which could model deformations of a wide range of surfaces. Energy minimization maintains a continuous surface, unlike coarse-grained models during which molecules can disassociate from the surface. Active matter can thus be consistently moved across energy minimal model surfaces. A coarse-grained model would require routines to determine which particles in the model form a closed surface before active matter could be moved along it.

It is worth noting that though the energy minimal method provides tractable analytical solutions to physics from kinematics to statistical mechanics, a generalized analytical framework for modeling deformable surfaces is out of

reach currently. Even provided if improbably one had the means to describe any possible manifold analytically, determining the minimal configuration and dynamic behavior on the way towards equilibrium would likely not be possible. Past energy minimal analytical descriptions of simple systems such as droplets, and chains have been limited to focusing only on static long-term behavior of the system[6, 5]. In an energy minimal description of lipid tethers numerical simulation was the only means to determine the static configuration of the tethers [24]. As will be shown in the following section on liquid modeling in Morpho 1.2.3, only semi-analytical solutions were found to static liquid deflections. All told, while not provably impossible, how one would create an analytical dynamic model of arbitrary deformable surfaces is unclear.

1.2.2 Morpho energy minimization:

The programming language Morpho was chosen as the means to model deformable surfaces coupled with active matter as it provides a platform to explore the dynamics of arbitrary deformable surfaces. As aforementioned, an analytical treatment of this problem is not possible, and thus a computational model is the only other means to generate theoretical predictions. Morpho allows the user to input a triangulated mesh, a series of points called vertices connected by lines called edges, without regard to its shape. This mesh, defining the surface of interest to the user, can then have energies such area, Gaussian curvature, mean curvature squared, and line tension applied to any region of the mesh. Within Morpho all of said quantities, as well as volume, can be listed a constraint, which will be to linear order locally constrained. Morpho then allows the user to relax their surface, i.e. minimize the energies selected on their mesh, subject to the constraints they enumerated. Further any vertex point of the mesh can be constrained to not move.

Two examples of how Morpho is used are illustrated below in figure 1.2.1. In 1.2.1a an initially ellipsoidal mesh is added to Morpho, area energy is applied to the system, volume is listed as a constraint, and then it was relaxed repeatedly until reaching the expected spherical equilibrium state. Within figure 1.2.1b the same ellipsoid is relaxed by minimizing area and mean squared curvature energies subject to the same volume constraint. This converges to an equilibrium configuration which is also spherical. This satisfies the area and mean squared curvature minimization as provided it is in a spherical configuration, the mean curvature for a sphere is $H = \frac{1}{R}$ where R is the radius of the sphere. Thus the integral of the energy of 1.2.1b $\int \frac{k}{2} H^2 dA + \int \sigma dA = 2\pi k + 4\sigma\pi R^2$ which can not be minimized any further than can 1.2.1a's energy $\int \sigma dA = 4\sigma\pi R^2$ subject to a volume conservation constraint. Thus Morpho replicates the result that the equilibrium configurations of 1.2.1b and 1.2.1a are the same.

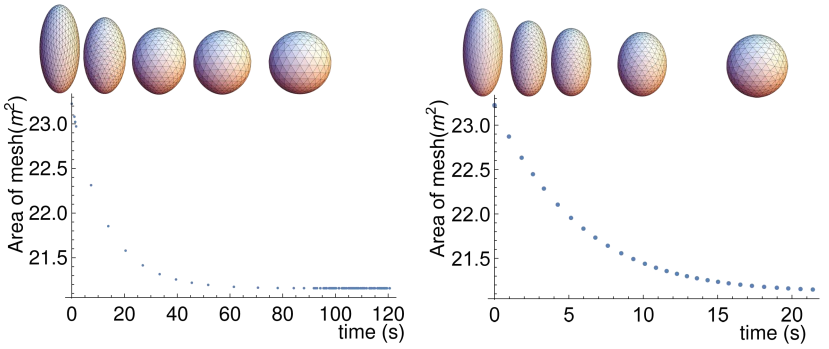

(a) Minimizing area

(b) Minimizing area and mean squared curvature

Figure 1.2.1: Morpho relaxing ellipsoidal droplet subject to volume constraint

In the examples above, as in all Morpho simulations, each relaxation step taken to minimize the potentially constrained energy functional specified by the user is calculated using a technique known as steepest gradient descent. Numerical Recipes defines a technique called steepest gradient descent which

accepts an energy functional $f(\vec{P_i})$ to be minimized which depends on $\vec{P_i}$, an element of vector space V. This method accepts an initial $\vec{P_0}$, and finds the value of $\vec{P}$ which minimizes f by alternating between finding the direction of local motion which will minimize f, and then moving in that direction. This update occurs simply by $\vec{P}_{n+1} = \vec{P}_n - \lambda \nabla f(\vec{P_n})$ [25]. This process ceases once f reaches a predetermined equilibrium condition. This technique exploits the fact that the energy functional given defines a multidimensional landscape whose height depends on its location in V. Moving to position $\vec{P}_{n+1}$ is moving in the direction which in $f(\vec{P_n})$ is locally falling the fastest towards $f = -\infty$.

Morpho uses a very particular formulation of steepest descent which moves many vertices via gradient descent based on local energies. During a given relaxation step let us consider vertex $\vec{v_i}$ which is a part of l faces $\vec{f}_{\vec{v}_i} = \{f_1, ..., f_l\}$, each with defined energies, and constraints labeled $E(f_j)$ and $C(f_j)$. For the vertex $\vec{v_i}$ the path which minimizes the energy of each face it is connected to $f_j \in \vec{f}_{\vec{v}_i}$ can be calculated via the steepest gradient descent form: $\vec{F}_{f_j}^{\vec{v_i}} = \frac{\partial E(f_j)}{\partial \vec{v_i}}$. The maximum possible change in energy of the conserved quantities for f_j caused by motion of $\vec{v_i}$ can be calculated via an analogous expression: $\vec{C}_{f_j}^{\vec{v_i}} = \frac{\partial C(f_j)}{\partial \vec{v_i}}$. If one repeats this process for all l faces for both minimization and constraint forces and adds the results together, one finds totals $\vec{F}^{\vec{v_i}} = \sum_{j=1}^{l} \vec{F}_{f_j}^{\vec{v_i}}$ and $\vec{C}^{\vec{v_i}} = \sum_{j=1}^{l} \vec{C}_{f_j}^{\vec{v_i}}$. In order to prevent $\vec{C}^{\vec{v_i}}$ from changing during the relaxation step, the total force applied to $\vec{v_i}$ is $\vec{F}^{\vec{v_1}} = \vec{F}^{\vec{v_1}} - \frac{\vec{C}^{\vec{v_i}} \cdot \vec{F}^{\vec{v_i}}}{\vec{C}^{\vec{v_i}} \cdot \vec{C}^{\vec{v_i}}} \vec{C}^{\vec{v_i}}$. As global minimization of a functional over a surface via this technique requires that local minimizations for each vertex described above work together, thus $\vec{v_i}$ is moved to $\vec{v}_{in+1} = \vec{v}_{in} - \lambda \vec{F}^{\vec{v_i}}$ where λ is generally a small real number called a length scale.

Other crucial aspects of Morpho include refinement, regularization, and length scale selection. For any mesh given to Morpho, there is a certain density

of vertex points per area of the mesh. The level of refinement is proportional to the density of vertex points per area of the mesh. Currently Morpho is capable of refining all of a mesh at a given time. Though refining a mesh increases the amount of time it takes to compute a relaxation step on it, it does increase the accuracy with which it can approximate a smooth curve. Regularization is an energy which can be added to a mesh which tries to equally space vertices from neighboring vertices, and have mesh faces have the same inner angles. This energy theoretically does not alter the minimization of other energies as it is confined to work in the null space of the discretized energy functional. Morpho can either perform relaxation steps with a given λ length scale, or select one in order to minimize energy via analyzing the system to find a length scale which will maximize energy loss.

1.2.3 Liquid deformation modeling with Morpho:

Liquid deformation will be modeled through minimization of the area energy functional. Any liquid in contact with a gaseous interface will attempt to minimize its surface area in contact with the perturbing gas. It is theorized that the liquid has negligible amounts of elasticity. Flowing media, liquids, which have appreciable elasticity will be referred as soft solids as they appear to exhibit distinct behavior from non-elastic liquids.

Both the ability of Morpho to converge with infinite time to the correct energy minimal configuration, and short time scale behavior will be tested in the following section. The ability of Morpho to model static liquid configurations will be compared to semi-analytical theory. Said semi-analytical model will be compared to recent quasi-static liquid deflection experiments. Morpho's modeling of liquids moving in time will be compared with power law relaxation behavior observed recently by experimentalists.

Posing an analytically solvable static test case:

Central and circular deflection of radius ϵ of height z_o in the z direction of a disk on radius $R > \epsilon$ in the x-y plane will cause symmetrical deformations about the z axis. As a result an analytical solution for the deflection of the disk as a function of distance from the origin in the x-y plane, ρ can be readily obtained. The full derivation of this solution, performed by Andrew DeBenedictis can be found in the first section of the appendix 4.1.

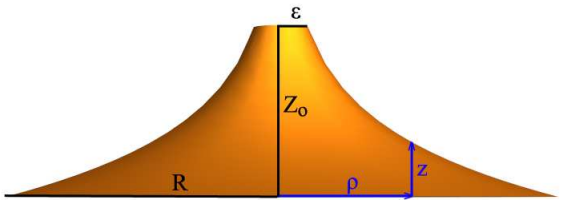

Figure 1.2.2: Parametrization of deflected area minimal disk

The full solution for height as a function of distance from the center, $z(\rho)$, for the configuration of the area minimal film connecting the outer ring and inner raised disk is a catenoid:

$$z(\rho) = \begin{cases} \rho \leq \epsilon & z_o \\ \rho > \epsilon & b - a \cdot \operatorname{arccosh}(\rho/a) \,|\, z(R) = 0, z(\epsilon) = z_o \end{cases} \tag{1.2.1}$$

We further discovered that, for a disk of radius R with a central deformation of width ϵ, the deformation must be of height less than zmax than to result in a static deformation.

$$\text{zmax}(\epsilon, R) = \epsilon \cdot \operatorname{arccosh}(R/\epsilon) \tag{1.2.2}$$

Since $\text{zmax}(\epsilon, R)_{\epsilon \to 0} = 0$ point deformations of area minimizing disk do not result in a stable configuration. This conclusion, as well as the catenoidal

solution have been independently derived by other researchers [24].

Comparison to static analytical test case:

Careful raising then immobilizing an inner region of a larger area minimizing disk is a means of reproducing the analytically solvable situation. The conformation of the disk, with a raised and fixed inner radius, to which it has converged after repeated calls to relax should be the stable configuration predicted by the analytical model. Incremental raising of the inner disk, paired with periods of allowing the rest of the disk to relax, brings the inner disk to the desired height while maintaining the accuracy of the relaxation routine. Once the inner disk reaches the final height, it is fixed and the whole disk is relaxed until convergence criteria are met.

In order to explore the agreement between the analytical solution and model created in Morpho above, a parameter set of 400 possible deformations were tested on a disk of radius 1 with $\sim 1566\frac{vertices}{area}$. A set of 20 evenly spaced deformation widths, ϵ, were tested. For each ϵ, 20 z_o values that result in stable configurations according to equation (1.2.2) were tested. For each parameter variation after the inner radius of width ϵ of the disk was brought to the height z_o and immobilized, the disks were relaxed. The relaxation process would continue until area changed less than 10^{-8} for 100 successive relaxation steps. Once converged, the distance in the x-y place from the origin, ρ, and height, z_o, for each vertex point in the mesh was recorded. For each run the unbiased sample uncertainty between all vertex z_o values and the z_o predicted analytically by the vertex's ρ value was computed. The results of this batch test is presented below in two graphs, one for large ϵ values and the other for small. The division of the plots serves to reduce the density of data points and that shows the agreement between Morpho and the analytical model follows a

similar trend when $\epsilon \to 0$ and $\epsilon \to R$.

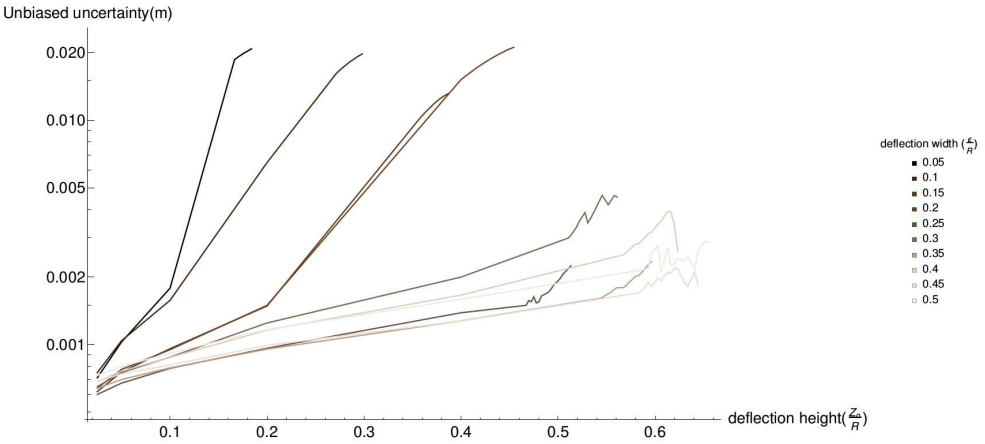

(a) Uncertainty of Morpho vertex positions for ϵ small relative R

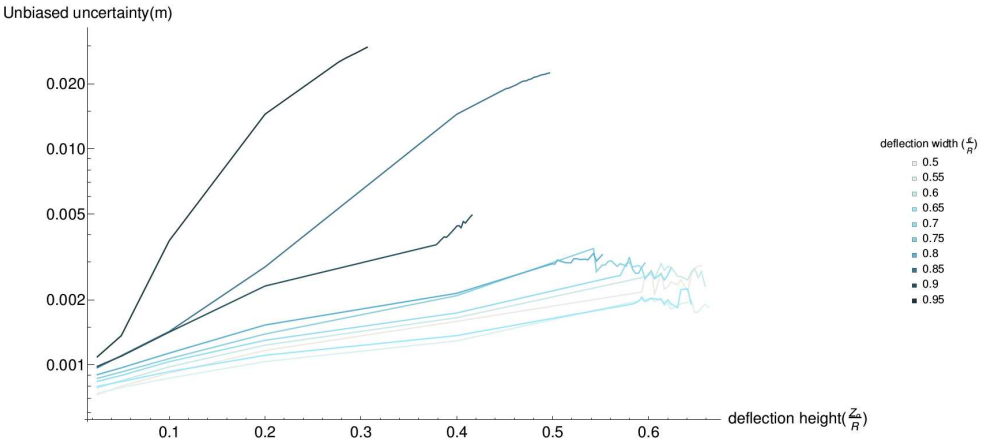

(b) Uncertainty of Morpho vertex positions for ϵ approaching R

Figure 1.2.3: Difference between analytical solution and Morpho

Morpho, for a wide range of deformation, is in excellent agreement with analytically predicted values. For $.2 < \frac{\epsilon}{R} < .85$, for all z_o values the uncertainty between the analytical solution and Morpho's results are $< .005$(m) and a disk 1(m) in radius. Morpho's capabilities to model area-minimizing deformations that are neither thin or extremely wide compared to the total size of the shape are sufficiently accurate for computational modeling. Clearly thin and wide

deformation are less accurate. Figure 2c) illustrates the final configuration of the least accurate run with an uncertainty of .0295 .

We theorize that the inaccuracy in runs outside $.2 < \frac{\epsilon}{R} < .85$ was driven by the discretization of the mesh. The region defined by $\frac{\epsilon}{R} \leq .2$ could refer to an area small enough that it contained relatively few vertices, thus forming a polyhedral raised structure instead of a raised disk due to the linear interpolation of the few points. Similarly it was reasoned that $\frac{\epsilon}{R} \geq .85$ would define an area large enough that only a few points would be relaxing between it and the outer radius. This would similarly result in an interpolation between the outer and raised inner radius resembling a linear piecewise function rather than a smooth curve. This was tested by running the most problematic run, $\epsilon = .95$ $z_o = 0.306496$ on a mesh with 3.95 times as many mesh points.

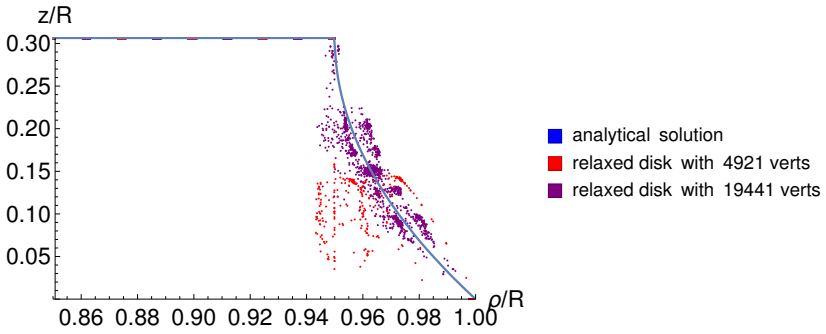

(a) z vs ρ for least accurate run compared to more refined run and analytical sol 1.2.1

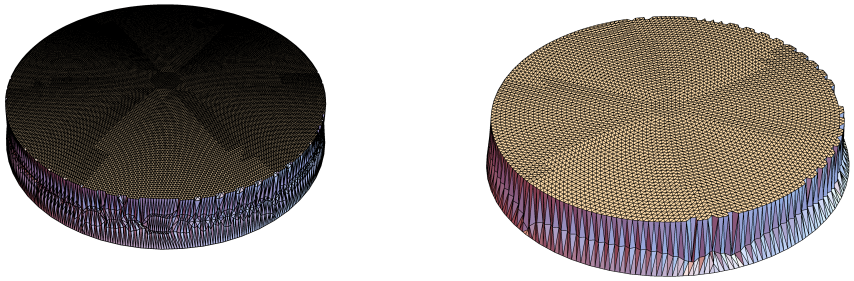

(b) Deflected disk mesh with 19441 vertices (c) Deflected disk mesh with 4921 vertices

Figure 1.2.4: Comparing problematic $\epsilon = .95$ $z_o = 0.307$ run with rerun on highly refined mesh

The results of refinement comparison clearly vindicate the suspicion that discretization drove error outside the $.2 < \frac{\epsilon}{R} < .9$ range. In fig 2a) the less refined run resulted in a very irregular distribution of points along the z axis. There are vertex points held along the raised inner radius, along the outer radius and a large cluster between $.15 < z_o < .05$. In Fig 2c) it can be noted that between the inner radius and the outer radius, there is a single line of vertex points. The more refined mesh's vertices formed a relatively even distribution of points along the slope of the analytical curve in 2a). This can additionally be confirmed visually in 2b), as there appear to be at least 3 vertex points connecting raised inner radius vertices to outer radius vertices.

Static comparison of analytical solution to experiment:

Having shown that Morpho and an analytical model agree closely over a wide range of parameters on the configuration of a constrained area minimal surface, it now remains to show that area minimization indeed models the deflection of liquids. The experimentalist Dr. Katharine Jensen at Yale university recently systematically recorded the deflection of liquids. Dr. Jensen's experiments will be compared to the analytical model via plotting area minimal analytical plots over her data.

Dr. Jensen tested the deflection of liquids in a manner which is, to a high degree of approximation, equivalent to the disk deflection detailed above. Starting with a dish of water several cm in radius and 300μm deep, Dr. Jensen probed the surface of the water using a rod with a spherical end point as shown below. After the sphere, of 24.5μm radius, was pushed below the surface and raised, the liquid stuck to it. She then slowly continued to raise the rod over several minutes so that the system quasi-statically evolved. At each time she

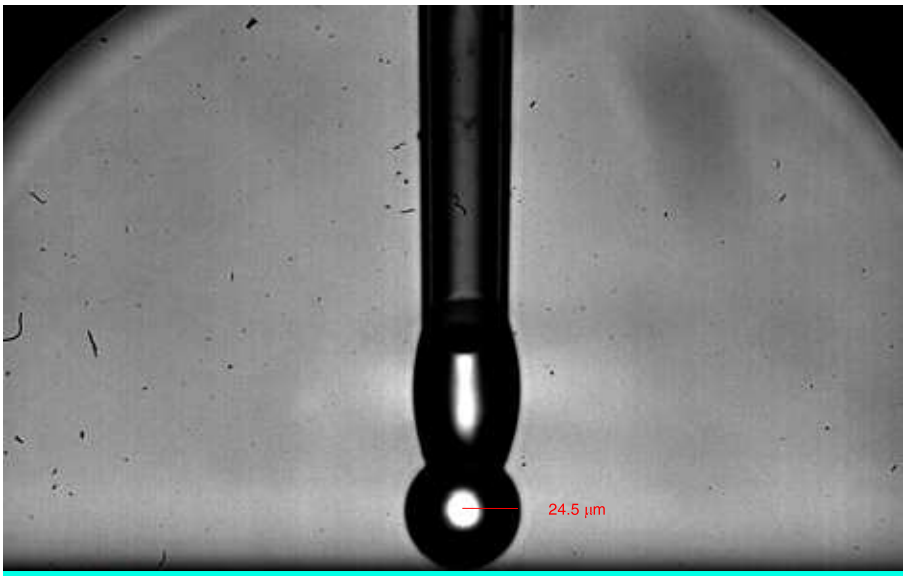

Figure 1.2.5: Liquid deflection experiment set up (Courtesy Dr. Jensen)

took pictures of the system, it appears the liquid forms a contact point with the rod with a known distance from the center of the bead, and height from the originally undeflected surface. Though the shape of the bead is spherical rather than flat as in the analytical model, the analytical model ought to be able to approximate the deflections measured if liquids can indeed be modeled by area minimal films. Between frames 20 seconds were let pass to allow the surface to reach equilibrium.

Below the comparison between area minimal catenary lines as calculated by Mathematica and Dr. Jensen's experimental data can be studied. For each frame a number of different solutions are shown, the solution forming the best approximation of the surface being underlined. Though the inner radius ϵ and height z_o are kept constant, the outer radius R of the solutions are varied. This is due to the fact of Dr. Jensen's camera about the deflection site making the ratios of ϵ to z_o known but either relative R unknown. As a result it is unknown precisely where the liquid's surface was at its undeflected height.

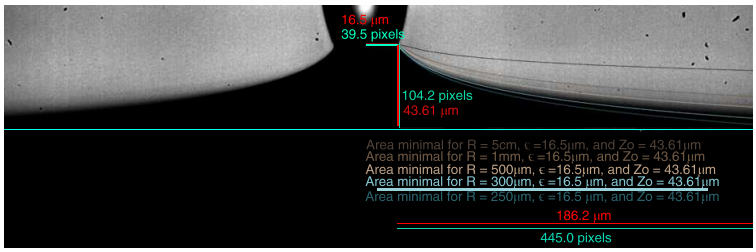

(a) frame 1 (Courtesy Dr. Jensen)

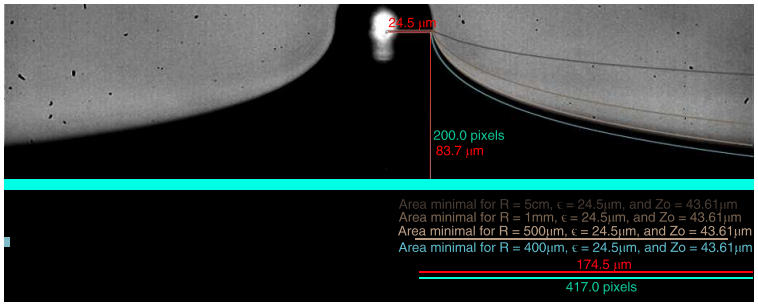

(b) frame 2 (Courtesy Dr. Jensen)

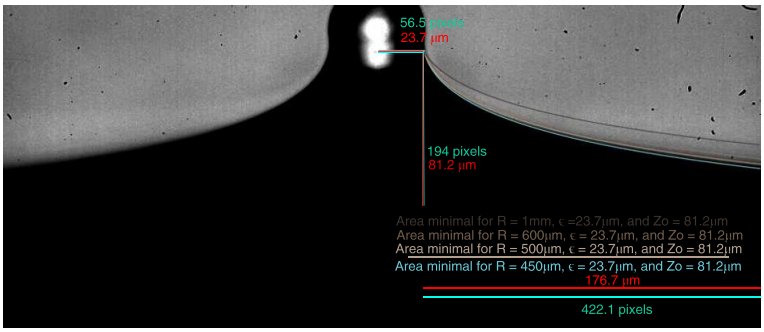

(c) frame 3 (Courtesy Dr. Jensen)

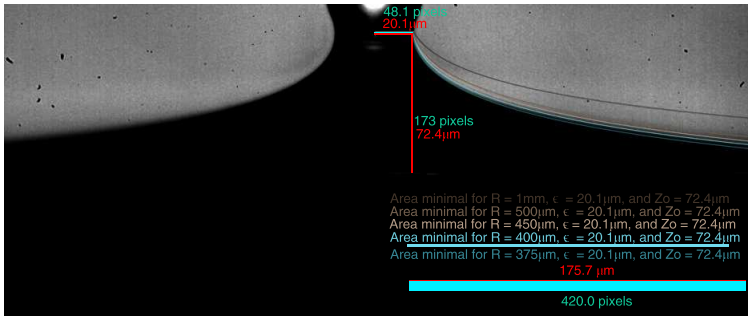

(d) frame 4 (Courtesy Dr. Jensen)

Figure 1.2.6: Static deflected liquids are area minimal configuations

As can be seen in the figures above, within all frames liquid deflection can

be approximated exceptionally well by an area minimal curve showing. The curves corresponding to the solutions underlined capture the curvature of the captured frames exceptionally well. These solutions can be observed to at first have an increasing outer radius, then shrink as the inner radius of the liquid contacting the bead shrinks.

While it might seem troubling that the area minimal curves do not correspond to the deflection being equal to 0 at the boundary of the dish, several cm away from the deflection, this indicates that the liquid has dipped slightly below its undeflected height along the outer boundary. Intuitively an area minimal curve must be area minimal between any two points along the curve. As can be seen in figure 1.2.7, zooming in on area minimal curve with an outer radius of several cm, as in Dr. Jensen's experiments, which dips below the undeflected surface closely about the deflection can be modeled by another area minimal curve. It would in fact be astonishing if the liquid, which is only 300 μm deep liquid sample allowed a ˜ 100 μm deflection form about the middle of the dish, with no corresponding decrease in height elsewhere in the dish.

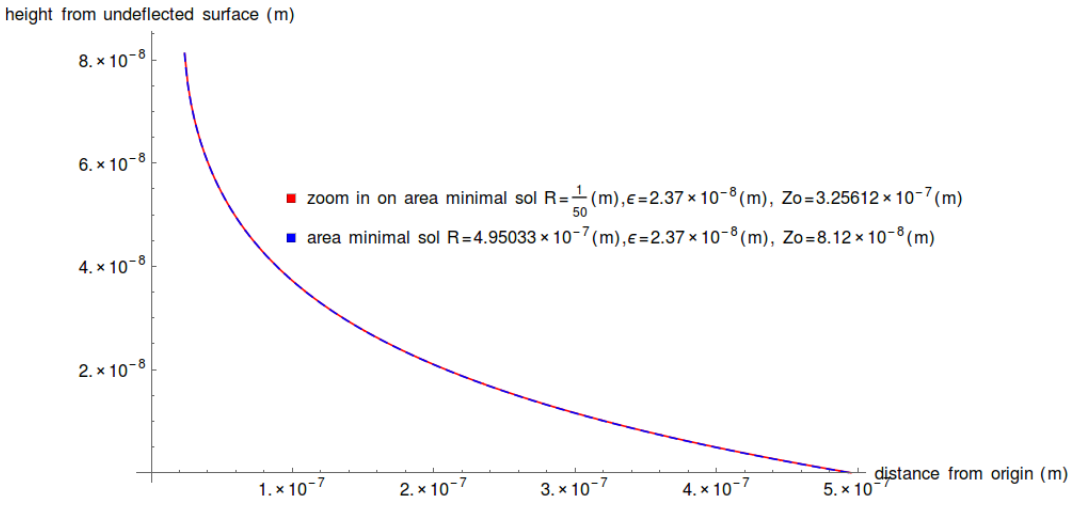

(a) Comparison between fit to in frame 3 to possible area minimal solution over whole dish

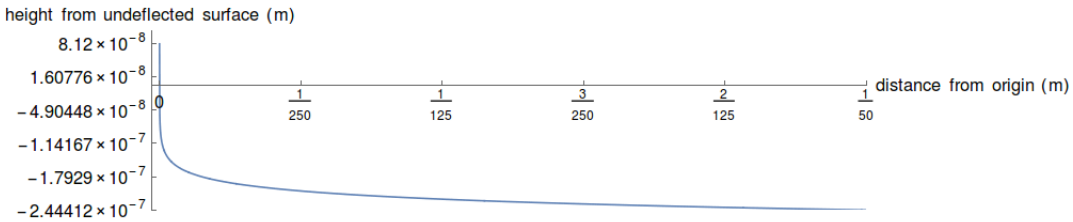

(b) Full view of extrapolated area minimal dish solution

Figure 1.2.7: Local area minimal fits shown represent plausible solutions over whole dish

Experimentally realized test case of liquid dynamics:

Dr. Jensen, in addition to recording the stable deflections of liquids, recorded the relaxation of liquid deflections back to equilibrium, and quantified this behavior. Using the same setup described above, Dr. Jensen continued deflecting the liquid until they broke off from the probe and rejoined the bulk. During these trials, frames of which can be studied below, Dr. Jensen observed that the max peak of the deflection, h_{max}, was proportional to $-\frac{1}{2}\ln(t - t_o)$ where t_o is the time at which data collection began.

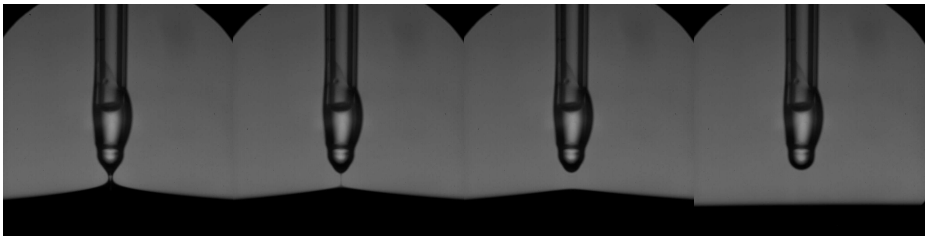

(a) frame 1 (b) frame 2 (c) frame 3 (d) frame 4

Figure 1.2.8: Relaxation of a deflected liquid (Courtesy Dr. Jensen)

While relaxing, deflected liquid surfaces exhibit two distinct relaxation phenomena. Firstly the inner contact point with the bead shrinks, while the bulk maintains a conical configuration. The bulk then, over a much longer time-scale relaxes completely its initial configuration. Unfortunately it remains unclear whether Dr. Jensen observed $h_{max}(t) \propto -\frac{1}{2}\ln(t - t_o)$ relaxation of the inner contact point, or the bulk.

Dynamic comparison of Morpho to experiment:

After having established that numerical area minimization captured the static behavior of liquid deflection and observed the experimental test case, it was

hypothesized area minimization is the leading factor determining the dynamics of the system. As in the limit of time approaching infinity Dr. Jensen's liquid deflections are area minimal, then area energy must be relatively one of the largest energies present in the system. While typically momentum is an important element of liquid systems, in the frames shown no oscillation are visible. Rather the deflection converges towards equilibrium. In the absence of other energies, or momentum it seems plausible that Morpho's gradient descent relaxation, which incrementally moves as directly as numerically possible towards equilibrium, ought to capture the dynamics of the system.

In order to best test this hypothesis catenoids with fixed outer boundaries were relaxed subject to area minimization. As the relaxing liquid deflections are initially catenoidal this was seen as good choice of initial state. Since Morpho cannot effectively run with the number of vertices required to approximate μm sized features on a cm dish mesh, the catenoids were made to be as fine as possible with $\frac{\epsilon}{R}$ about the value 0.05. These catenoids were raised by incrementally forcing an inner radius of points upwards to a final deflection height, z_o, even if it was energetically unfavorable. Catenoids were raised both to equilibrium configurations, ones in which $\text{zmax}(\epsilon, R) > z_o$, and those exiting equilibrium with values of z_o very near zmax. The $h_{max}(t)$ decay behavior of these simulations can be observed below.

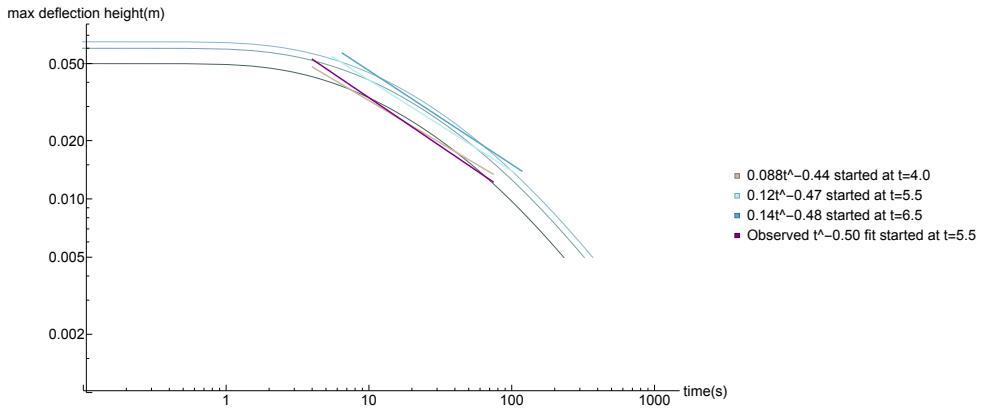

4

Figure 1.2.9: Relaxation of $\frac{\epsilon}{R} = 0.04$ for range of equilibrium z_o relaxes to $\frac{z_o}{2}$ according to $t^{-\frac{1}{2}}$

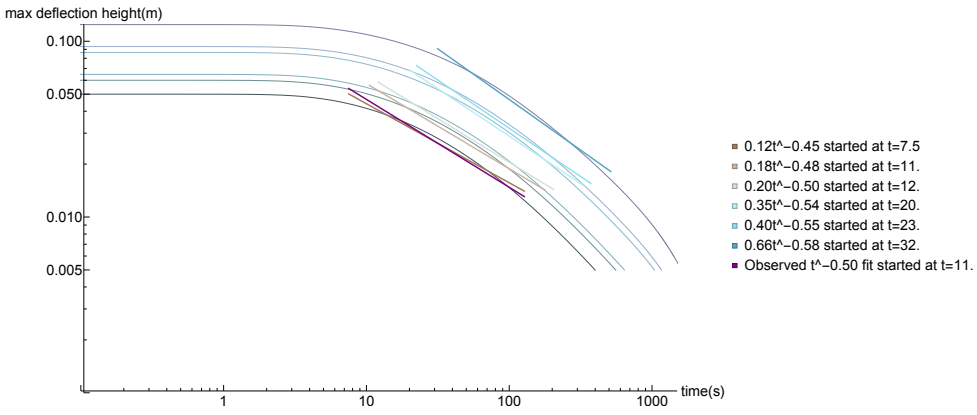

Figure 1.2.10: Relaxation of $\frac{\epsilon}{R} = 0.06$ for range of equilibrium z_o relaxes to $\frac{z_o}{5}$ according to $t^{-\frac{1}{2}}$

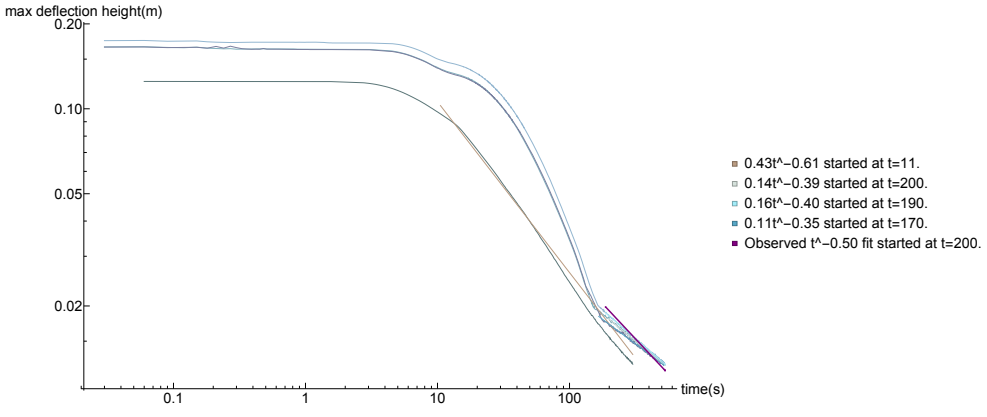

Figure 1.2.11: Relaxation of $\frac{\epsilon}{R} = 0.05$ for range of z_o near zmax $= 0.184$ for $z_o > .13$ obey $t^{-\frac{1}{2}}$ roughly once near equilibrium

The relaxation behavior $h_{max}(t)$ of area minimization simulations is sensitive to the initial dimensions of the deflection being relaxed. In figs 1.2.9 and 1.2.10, while the catenoid was in equilibrium the deflection decayed progressively faster as the simulation continued. On the other hand configurations which are nearing unstable fig1.2.11 appear to relax faster than those in equilibrium yet suddenly switch to a slower regime. The $h_{max}(t) \propto -\frac{1}{2}\ln(t - t_o)$ observed fit, to a good approximation for a vast portion of relaxation of equilibrium configurations, is not seen regardless of the initial conditions of the deflection. Deflections even in the equilibrium case, while the deflection is about its initial height z_o or 0 are not approximately proportionate to $-\frac{1}{2}\ln(t - t_o)$.

It is also clear from observing the $h_{max}(t)$ dynamics of area minimization, that Morpho's gradient descent routine length scale does not correspond directly

to change in time. When running these simulation time was updated after each step by adding the length scale λ i.e. $t_{n+1} = t_n + \lambda$. However using this update rule, Morpho claims that area minimal surfaces take many hundreds of seconds to fully relax. As area minimization is supposed to describe liquids, which relax on the scales of fractions of a second, this indicates either that liquids are dynamically not area minimal, or that Morpho's length scale λ does not correspond to a change in time directly.

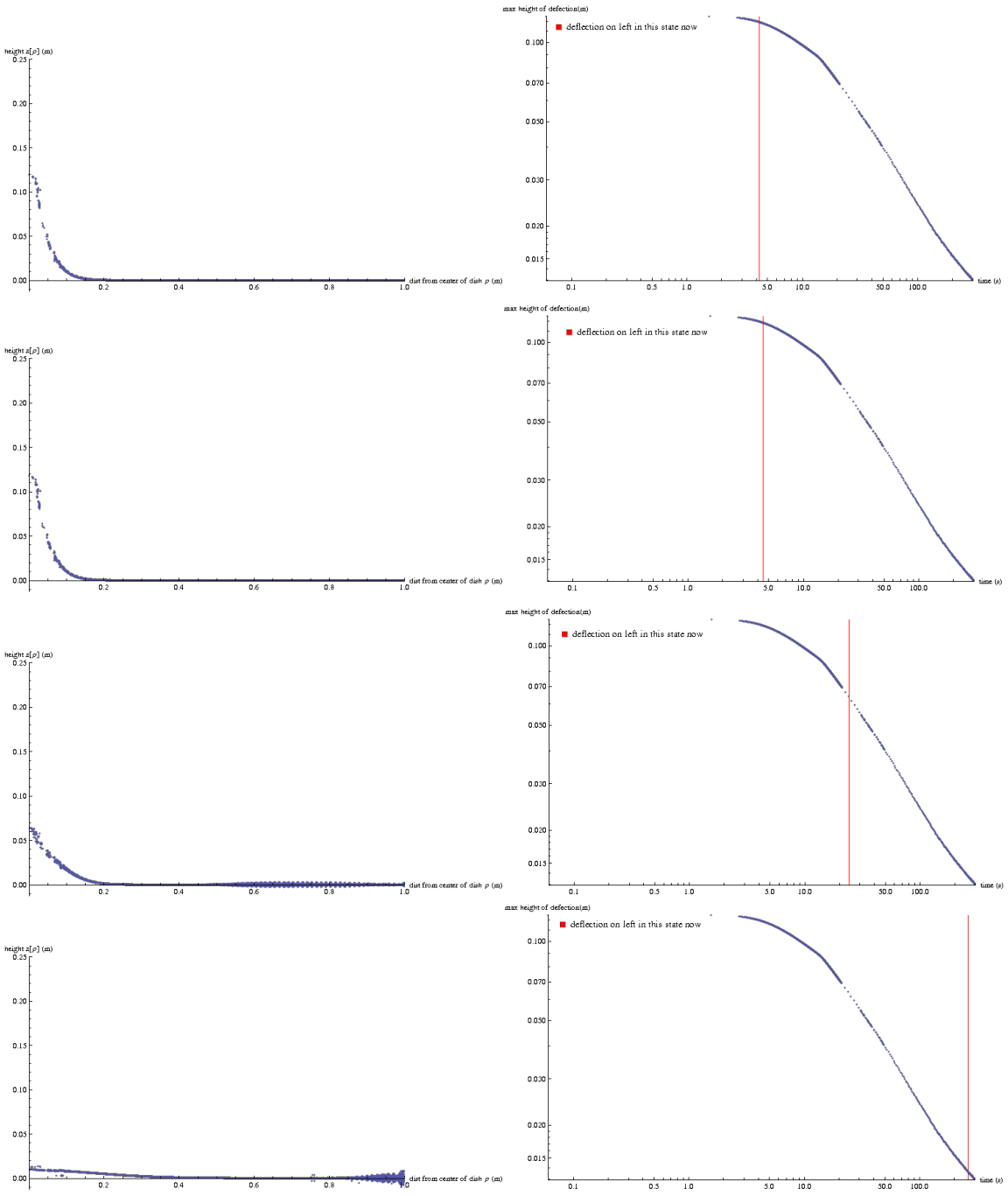

Figure 1.2.12: Frames from relaxation of $\frac{\epsilon}{R} = 0.05$ and $z_o = 0.125$ show behavior unlike experimental frames sent 1.2.8

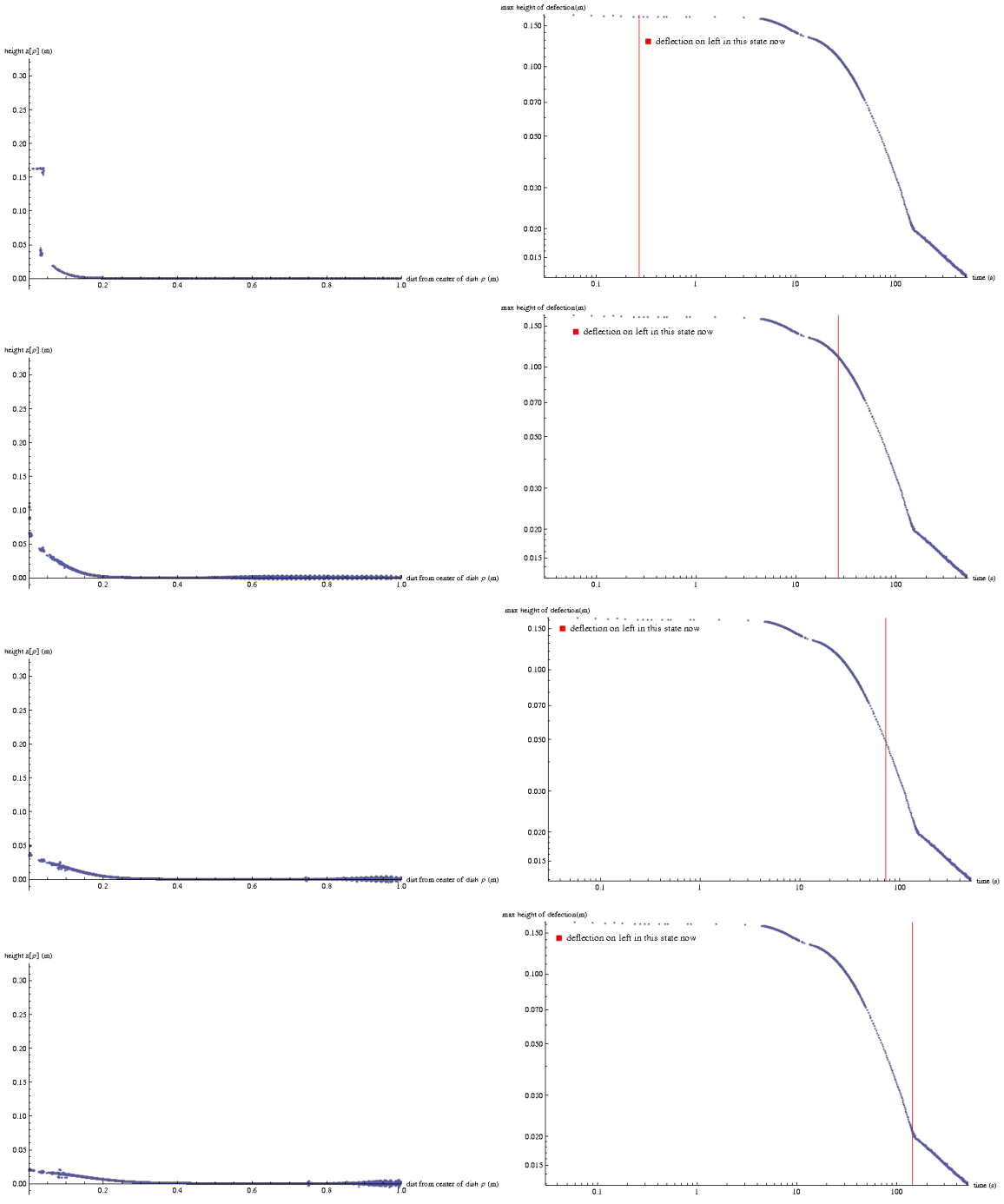

Figure 1.2.13: Frames from relaxation of $\frac{\epsilon}{R} = 0.05$ and $z_o = 0.1625$ show behavior experimental frames sent 1.2.8

Visualizations of the deflection relaxations elucidate the source of the relaxation slowdown transition of unstable configurations and suggest unstable configurations were those tested by Dr. Jensen. The relaxation of equilibrium

configurations shows a single deflection about $\rho = 0$ diffusing into the bulk. Unstable deflections become more thin about the middle of their height than at h_{max} just as in experiments and shrink to a minute radius film connected to a linearly deflected bulk. This behavior mirrors remarkably well what has been observed in Dr. Jensen's experiments as shown in figure 1.2.8. In simulations once this minute film joins the bulk, h_{max} is proportional to between $t^{-.4}$ and $t^{-.5}$ similar to equilibrium simulations. Thus in a sense there are multiple relaxation processes happening, an inner deflection relaxing atop a larger deflection relaxing at a slower rate.

Direct viewing of relaxation frames further corroborates that a fixed outer boundary may be a fundamentally flawed assumption for simulating liquids but not one which changes the dynamics immensely. Whether in equilibrium or unstable initially, progressive area minimization caused ripples in the surface. These ripples form across the whole mesh, but then gravitate towards the fixed boundary where they increase in amplitude. This indicates that area minimization is trying to raise or lower the outer most section of the mesh repeatedly, however is being prevented from doing as as the outer boundary is fixed. Yet the overall behavior observed by Dr. Jensen was seen, thus it would be foolish to rule out the simulation predictions that for liquids $h_{max}(t)$ can be locally approximated about chosen values of t using power laws, and sudden $h_{max}(t)$ changes are due to features being absorbed into the bulk.

1.2.4 Soft solid deformation modeling with Morpho:

Static comparison of Morpho to experiment:

In the same manner which Dr. Jensen tested the quasi-static deflection profiles of liquids via slowly deflecting them, Dr. Jensen experimentally observed the

deflection profiles of soft solids. Using the same setup as used with liquids, Dr. Jensen replaced the water in the dish with water containing the polymer PDMS, polydimethylsiloxane. The polymer PDMS is anisotropic, and cross-linked thus providing elasticity to the liquid it is a part of [15]. The resulting static deflections were far more peaked than their liquid counterparts.

Mean squared curvature and area minimal static configurations are shown alongside the static soft solid frames. For a given frame the ratios of ϵ, z_o, and R were measured within Photoshop. Then in Morpho configurations generated by maintaining the ratios of ϵ and z_o, while varying R were tested. Like in the case of modeling liquids, the ratio of ϵ and z_o was maintained for varying R. This allowed testing of these deflections in Morpho despite Morpho's inability to capture μm features while also showing the effect of increasing R towards configuration closer to those tested. The configurations for a chosen set of parameters were generated by inputting an initially undeflected dish mesh, fixing the outer boundary, raising an inner portion of the mesh, and then relaxing the mesh in this deflected position. The raising process was done by moving the mesh up to z_o in two moves, while minimizing only area energy. Slower movements upwards or the inclusion of mean squared curvature energy during this process caused numerical instability. The disk once fixed was relaxed until its energy changed by less than 10^{-6} for 50 consecutive iterations.

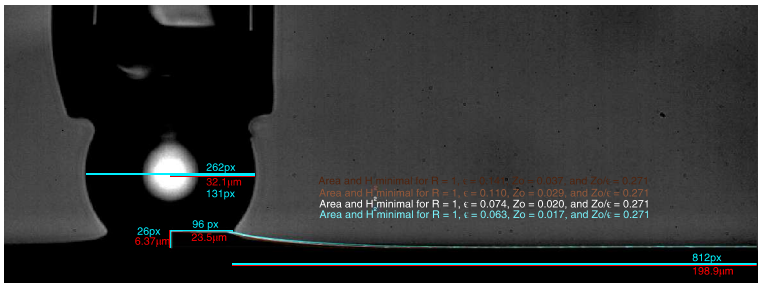

(a) frame 1 (Courtesy Dr. Jensen)

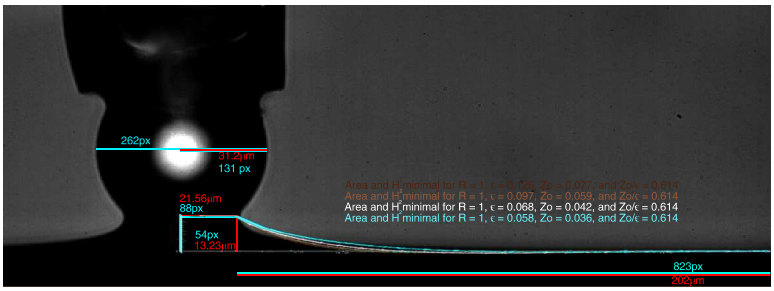

(b) frame 2 (Courtesy Dr. Jensen)

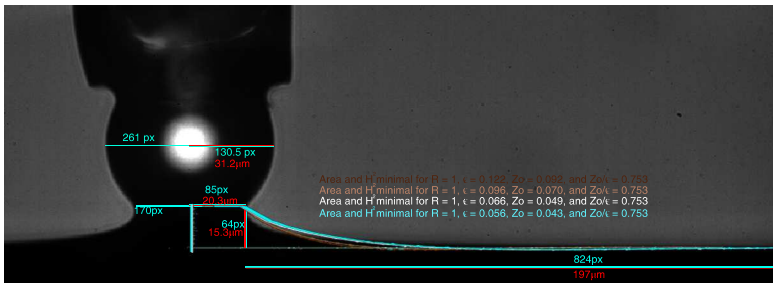

(c) frame 3 (Courtesy Dr. Jensen)

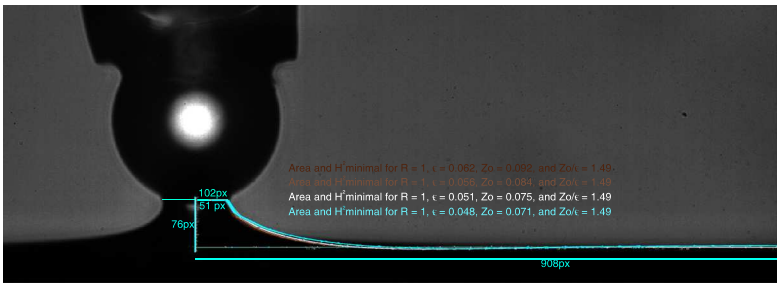

(d) frame 4 (Courtesy Dr. Jensen)

Figure 1.2.14: Static deflected soft solids are approximated by area and mean minimal squared curves

Morpho's minimization of mean squared and area energies provide an approximations about experimental results, however not as well as Mathematica's area

minimization approximated liquids. While catenary curves were always found to fit to liquid deflection profiles, all attempted solutions fail to capture the full curvature of frames 2 and 3. Also all area and mean squared minimal solutions shown dip below the undeflected surface, albeit to varying degrees.

The approximations in Morpho ought to be less accurate than Mathematica's area energies minimization approximations of liquids. Firstly the use of Morpho required deflecting an initially flat mesh with a fixed outer boundary, then relaxing down. As a result the simulations in Morpho physically represented deflection of a dish where liquid was added to the system at the same rate as a volume of deflected surface was forced form the bulk. More importantly however is the fact that now that two energies are active in the system, mean squared curvature and area, the ratio of the two may be essential to capturing even the statics of a given soft solid surfaces modeled by these two energies. Morpho currently only allows users to minimize these quantities with equal magnitudes.

Experimentally realized test case of soft solid dynamics:

Dr. Jensen thoroughly tested the dynamic relaxation behavior of a soft solid surfaces, providing an excellent test case. Dr. Jensen deflected a soft solid using a bead, and raised the bead until the contact point of radius $1\mu m$ and height $20\mu m$ between the soft solid and the bead broke. She then recorded the relaxation of said contact. Unlike in the case of liquids, Dr. Jensen observed $h_{max}(t) \propto -\frac{2}{3}\ln(t - t_o)$ relaxation of the maximum height of the deflection, h_{max}, in time. Frames of this relaxation process are shown below.

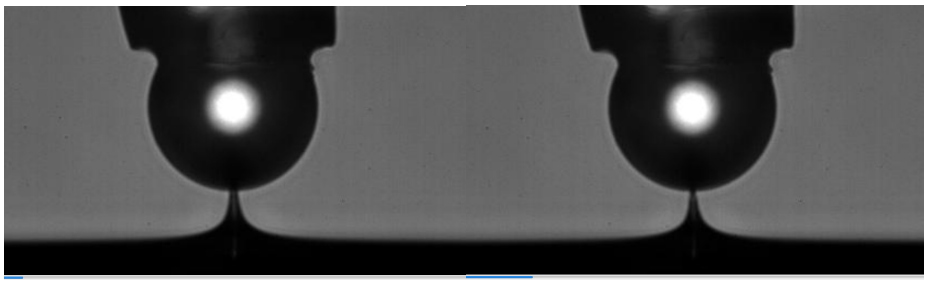

(a) frame 1

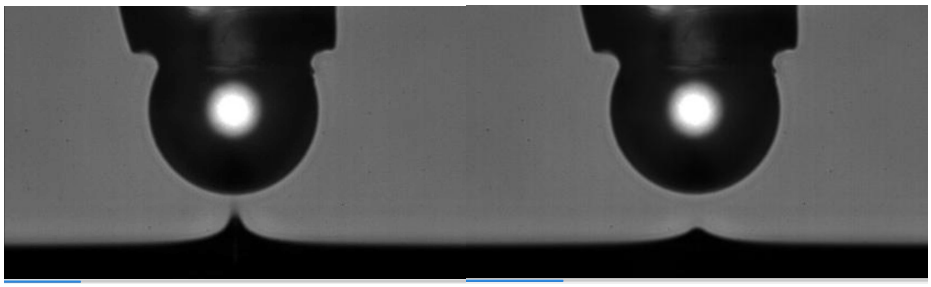

(b) frame 2

(c) frame 3

(d) frame 4

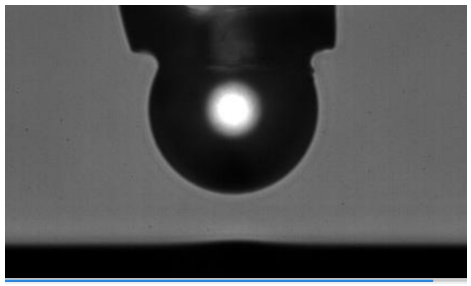

(e) frame 5

Figure 1.2.15: Relaxation of a deflected soft solid (Courtesy Dr. Jensen)

The relaxation of soft solids is clearly localized, and distinct from liquid relaxation. Unlike liquid deflection relaxation, during which the contact became thin before seemingly disappearing, the soft solid contact remains thick and visible during its relaxation. Further Dr. Jensen confirmed that the outer portion of the soft solid relaxation frames have not changed from their original undeflected height. Thus soft solid relaxation is a localized phenomena, unlike liquid relaxation which involves the whole bulk.

Dynamic comparison of Morpho to experiment:

As a means of further testing the hypothesis that mean squared curvature and area minimization determine the dynamics of soft solids, an attempt was made to replicate the experimental relaxation behavior of soft solids with Morpho. In spite of lacking volume conservation, or a specific ratio of the two energies, mean squared curvature and area energy minimization with Morpho did compare statically quite well to experiment. Agreement between experimental dynamic results and Morpho simulations would further clarify whether mean squared curvature and area energies are the chief contributors to the dynamics of soft solids.

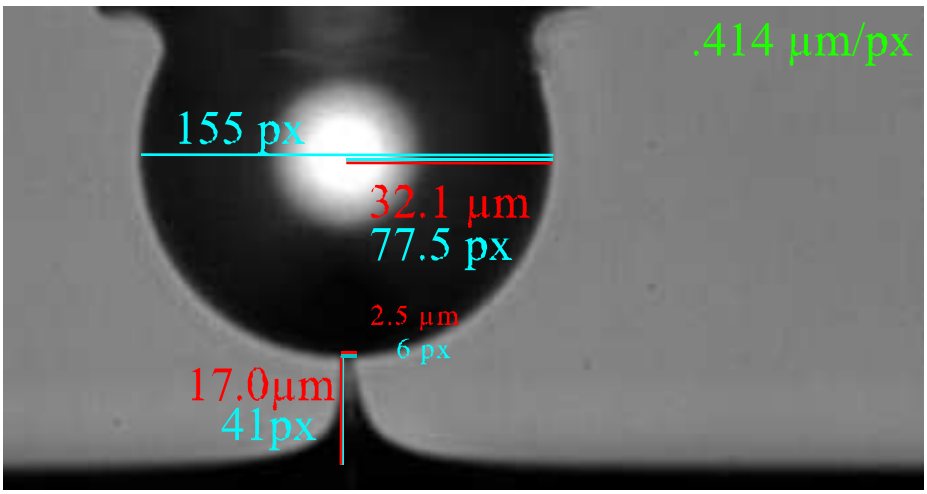

Figure 1.2.16: Measurement of deflected soft solid just before detachment (Courtesy Dr. Jensen)

To model the relaxation of soft solids, sharp deflections with fixed outer boundaries were relaxed via area and mean squared curvature energies. Unlike in the case of liquids, initial states were not made to be catenoidal. Experimental images reveal that before relaxation soft solid deflections are not stable catenoids, but instead highly peaked symmetric tubes with a catenoid-esque attachment

to the bulk. Before becoming unstable soft solids reach a ratio of inner radius to height, $\frac{c}{z_o} > 16$ as can seen above in figure 4.1.0.5. Though the inner deflection is incredibly fine, the relaxation of the feature occurs over a similarly minute portion of the total bulk 1.2.15. Thus modeling these features on a substantially smaller disk was seen as reasonable. Tests were performed about as small an inner radius as possible $0.025 = \frac{c}{R}$ to minimize the influence of the fixed outer boundary. The intensely peaked pre-relaxation states were approximated in Morpho by incrementally forcing an inner radius of points upwards to a final deflection height, z_o, even if it was energetically unfavorable in only 2 steps, and relaxing slightly after each step. Then the inner radius was released, and the max height of the deflection was measured over time.

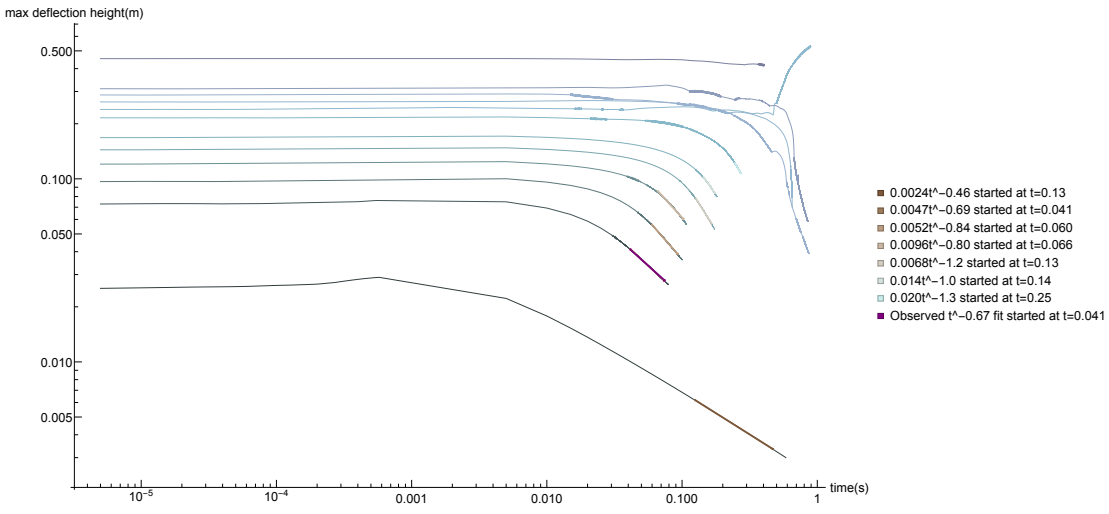

Figure 1.2.17: Relaxation of wider ($\frac{c}{R} = 0.05$) deflections shows meta-stability followed by descent

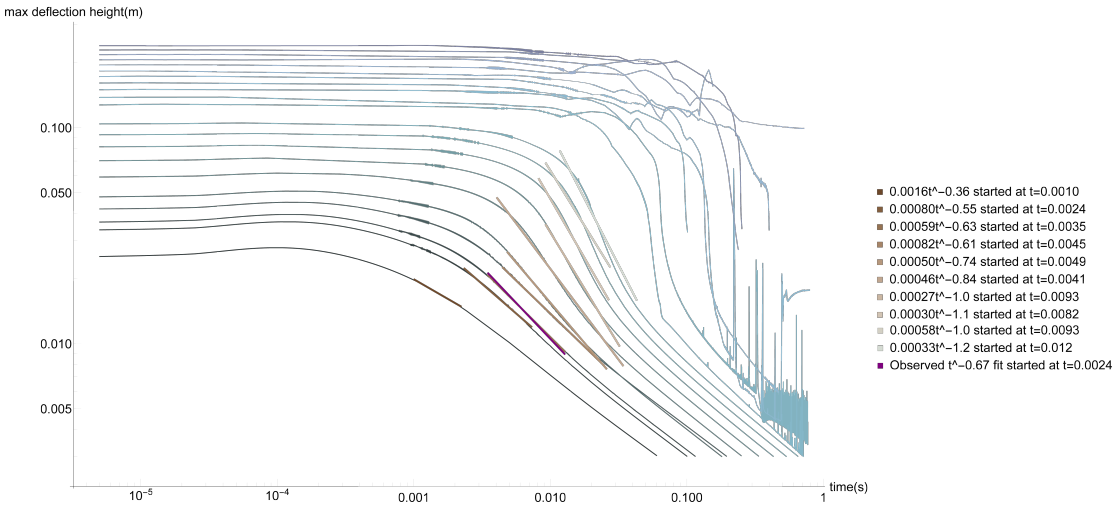

Figure 1.2.18: Relaxation of thinner ($\frac{\epsilon}{R} = 0.025$) deflections show acceleration and deceleration phases of relaxation

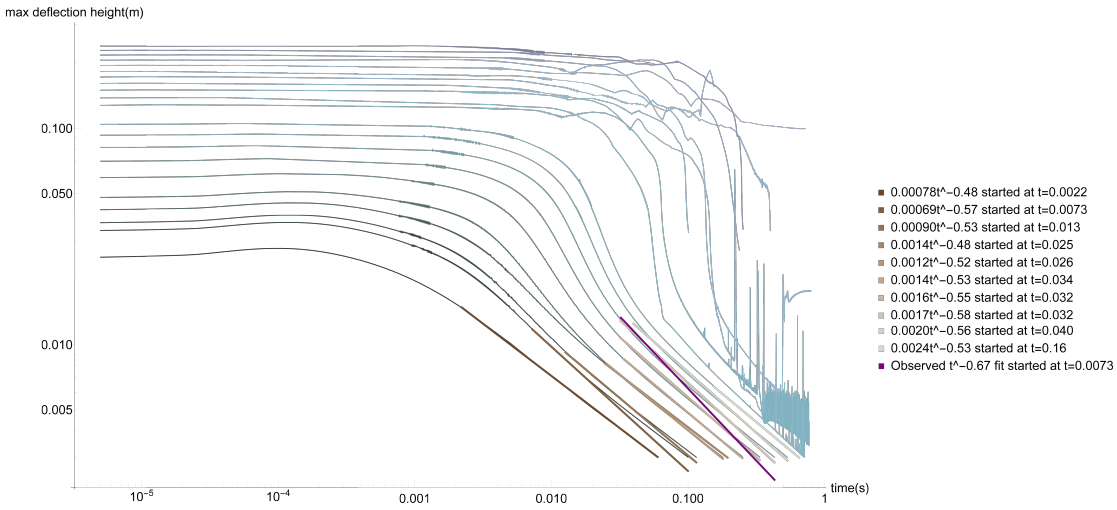

Figure 1.2.19: Relaxation of thinner ($\frac{\epsilon}{R} = 0.025$) deflections show acceleration and deceleration phases of relaxation

Relaxation of deflected area and mean squared curvature minimal structures results in meta-stability and a range of power law decay behavior. Intriguingly the more peaked a deflection, the more resistant it was to beginning to relax. This is in agreement with established analytical work which predicted the inclusion of mean squared curvature minimization to area minimization results in meta-stable configurations [24]. Also once mean squared and area minimal

structures begin to relax, they always cease to relax faster after a certain point. This is in stark contrast to pure area minimization which resulted in seemingly unbounded acceleration of h_{max} decay in time, slowing only temporarily as features were absorbed into the bulk. As a consequence area and mean squared curvature minimization results in stretches of true power law $h_{max}(t)$ behavior. However these power laws are of a variety of values, not strictly the observed $h_{max}(t) \propto -\frac{2}{3}\ln(t - t_o)$.

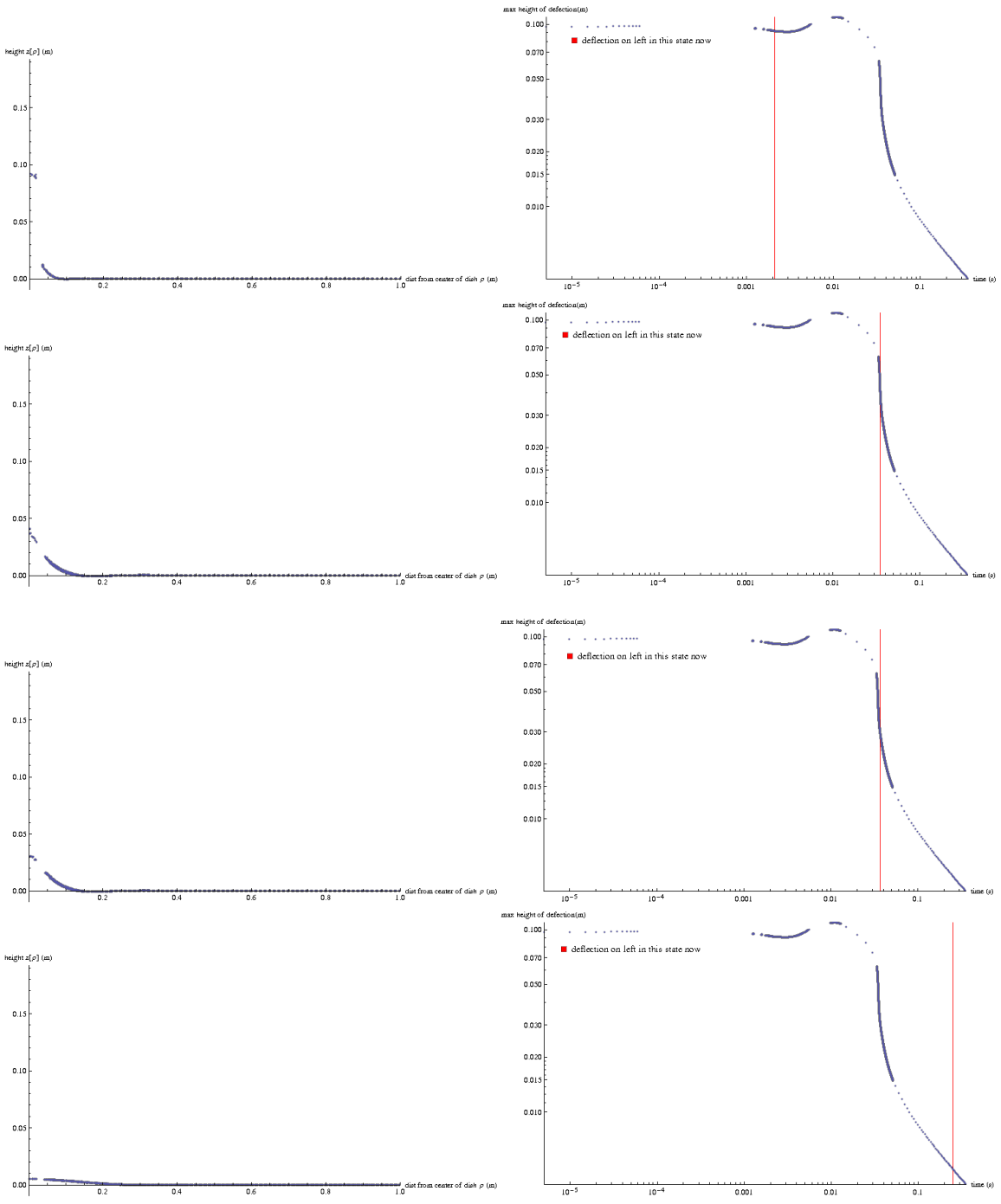

Figure 1.2.20: Area and mean squared minimization of deflection with $\frac{\epsilon}{R} = 0.025$ and $z_o = 0.096$ shows localized relaxation (Courtesy Dr. Jensen)

Direct study of simulations shows mean squared curvature and area minimizing deflection dynamics compares well to experimental soft solid predictions.

Deflections relaxed via minimizing mean squared curvature and area result in a lump relaxing about $\rho = 0$ whose max height approaches 0. Relaxation causes this bump to maintain a distinctly domed top, as in Dr. Jensen's experimental observed frames in fig 1.2.15. Finally this relaxation process occurs over the scale of a tenth of a second, a physically plausible time-scale.

1.3 Numerical energy area and mean squared curvature minimization as means of modeling deformability:

Simulation work with Morpho and Mathematica's numerical minimization schemes has shown that area and mean squared curvature minimization has immense potential for modeling deformable surfaces of interest. When compared to static experiments, these methods have been shown to produce remarkably similar configurations. In addition these numerical models, in the static case, are based upon solid theoretical footing. In the same manner springs with defined elasticity deform in response to minimize, surfaces with well-defined areas and curvatures ought to move to minimize them if increases in said quantities cause the system to become more energetic and perturbed. Liquids and soft solids respectively can be argued to have area and area and mean squared curvature energies as their interfaces are energetic and elastic. Due to the ease of posing analytically unsolvable minimization statics problems relevant to deformable surface modeling and excellent comparison to experiment, numerical minimization could be counted on as a tool by future researchers attempting to model deformable surfaces.

Dynamic behavior of Morpho's steepest gradient descent minimization rou-

tine and experimental results has provided replication of the phenomenology of liquid and soft solid dynamics, yet operates on time scales which are not readily comparable to current experimental data. Morpho minimization of deflections made closely approximate to observed soft solids and liquids configurations before deatchment has resulted in replication of the distinct forms of these two relaxation processes. Yet though at times Morpho replicated experimental predictions of $t^{-\frac{1}{2}}$ liquid relaxation and $t^{-\frac{2}{3}}$ soft solid relaxation, they were by far not the only relaxation behaviors observed. In the case of liquids this behavior was only seen in area minimal surfaces near equilibrium for the majority of their descent, or after an unstable liquid's thin film collapsed into the bulk. It is still unclear as to whether experimentally $t^{-\frac{1}{2}}$ relaxation was observed of the film, bulk, or both. Similarly the $t^{-\frac{2}{3}}$ relaxation was observed, but seemed predominantly to be the behavior of soft solids after their most peaked feature had collapsed on a faster time-scale.

A lack of robust theoretical explanation for why Morpho would replicate experiments clouds these dynamic results as well. Simple gradient descent based upon the update of the positions of the mesh vertices via $\vec{v_i}_{n+1} = \vec{v_i}_n - \lambda \vec{F}^{\vec{v_i}}$ may not theoretically, and in the case of liquid experiments certainly not , correspond to a change in time $dt = \lambda$. The Lagrange formulation of the principle of least action, which is used rather than minimization of available energies to fundamentally model the time evolution of energetic systems, is based upon minimizing of all ways that a system have kinetic energy minus all the manners in which it can have potential energy via $\mathcal{L} = \sum_{i=1}^{N} \frac{\dot{q}_i^2}{2m_i} - U_i$. Gradient descent minimization of $\mathcal{L}$ for the potential area with no possible kinetic energy resulted in similar dynamics to Morpho's area minimization, but on drastically more reasonable time scales in appendix entry 4.3. Thus while it is promising Morpho replicates experimental phenomenology, and predictions

of power law descent behavior, it cannot be assumed to be capable of accurate dynamic predictions yet.

In order to clarify how steps taken in Morpho correspond to changes in physical time and thus produce reliable dynamic predictions, clearer experimental predictions will be required. Simulations have predicted a range of relaxation behavior should be observed for the relaxation of soft solids and liquids. These predictions are well-motivated as they predict faster h_{max} relaxation when multiple parts of the deflection, and bulk are all relaxing simultaneously than when they have combined. Clearer articulations of when certain power law behaviors were observed is thus essential to comparing simulations to experiment. At present a dearth of such information has made proving whether Morpho's steepest gradient descent is capable of capturing the dynamics of liquids or soft solids problematic. Additionally equipped with said information other models based upon action minimization, rather than energy minimization, could be rigorously compared to experiment.

In its current form Morpho cannot minimize surfaces which can vary along smooth surfaces, such as containers or deflecting probes thus potentially preventing it from accurately modeling deformable surface dynamics. By posing a problem as an over damped energy minimization problem, one has stated that the system will surge towards a stationary equilibrium position as fast as possible. For such a system to act dynamically, thus requires the system to have already left equilibrium. In its current state Morpho can only allow vertices along a surface to move to minimize the energies assigned to it, or remain completely stationary. In reality minimization problems of a functional $f(\vec{x})$ defined over an N dimensional space H (i.e. $\vec{x} \in H$) can be confined to slip along only curves specified by $\vec{\phi}(\vec{x})$, called transversality conditions. An example of the such a system is a chain attached to two poles of arbitrary

smooth geometries [6]. In the case of the deformable surfaces Dr. Jensen tested, the surfaces freely deformed along a probe poked into the surface, and along the edges of the dish.

A potential explanation for the long time-scale non-power law behavior of liquid modeling through area minimization is that area minimization needs transversality conditions in order to capture the dynamics of liquids which spread deflections across the bulk in a small volume dish. In order to correctly model the soft solid experiments transversality conditions are theoretically not required as the deflections did not spread across the entire bulk to change the initial deflection of the dish as far as we know. This distinction could explain the discrepancy between the success of modeling liquids and soft solids in Morpho rather than a fundamental problem with how Morpho simulated over damped relaxation of energetic surfaces.

Inclusion of such transversality conditions to Morpho would be remarkably easy to accomplish. At each time step the negative gradient of the energies of vertices with specified transversality conditions could have any component of their energies which would move them perpendicular the curve they are confined to travel along subtracted. One method of implementing this would the user to select points and force them to only along a mathematically defined curve in 3-D space. Similarly another implementation could allow the user to select points and force them to only slip along the surface of another triangulated mesh.

Chapter 2

Active Matter:

Moving biological systems universally move by correlated motion of many independent components. Bacteria, birds, fish, and humans when moving in groups together form patterns which, while guided by the potentials around them, are determined by the interaction of neighboring constituents. Unlike isolated charges, masses, or commonly studied equilibrium statistical ensembles whose motions are determined solely in response to their environments, biological systems appear to be also guided by local organization of the system itself. Consequently biological systems can walk up flights of stairs, or organize into flocks rather than simply remaining in configurations which minimize exposure to external potentials. This leads to a seeming dichotomy between animate biological systems, and inanimate ones commonly studied in physics.

Recently a framework for quantifying mathematically the motions of biological systems, and equivalent inanimate systems, has begun to take shape under a field labeled active matter. This field is unified in its focus of studying the evolution of systems, in a wide range of different confinements, of constituents which use energy to locally promote specific alignment and motion of neighboring constituents [20]. The propensity for alignment in active matter systems

have been divided into polar, and nematic. Polar active matter constituents align to the mean direction of their neighbors. Active nematics describe the more general case in which constituents align to their neighbors via a tensor [19]. The confinements of active matter group active matter systems into dry and wet systems. This distinction is based solely upon whether the constituents are so heavily damped that momentum is not conserved in the case of a dry system, or conserved otherwise in a wet system [19]. The less understood case in which active matter is within a bulk with some elasticity will be discussed in chapter 3.

2.1 Established modeling techniques:

An abiding component of the study of active matter simulations has been the analysis of actor models of individual constituents interacting, either abstractly representing behavior of the system or directly modeling the components of the system. Active matter began in its current form from the study of minimal model of polar flocking. Said model , known as a Vicsek model, integrated forward in time distributions of points with constant velocities, in the direction of their neighbors given some noise. Within the Vicsek model a phase transition from a disordered chaotic states to an ordered state, where all particles move in the same direction, for low noise or high particle numbers was observed [33]. A Monte Carlo model was created to model the active nematic systems formed by microtubules being moved by kinesin motor proteins [32]. This model exhibited phenomenologically similar behavior to microtubule-kinesin systems by evolving the system based upon kinesin causing adjacent microtubules moving away from one another to speed up. A phenomenological model of the same system was composed of hard rods extending, then splitting. This model was able

to reproduce the experimental result that motor protein microtubule system defects align over long length scales [8].

Continuum theories of the evolution of active matter systems have created a rigorous mathematical framework for active matter which predict the results of actor models, and experiments. Continuum equations of polar active matter were derived starting from the XY model, in which neighboring particles posses direction which energetically align to the direction of neighboring particles, including a convective term to represent the non-stationary nature of the aligning particles[31]. A slight permutation of these continuum equations was found through deriving the hydrodynamic equations for standard Boltzmann statistical mechanics kinematic theory formulation of particles which align to the direction of a particle within a certain distance of them [3]. These two models respectively predicted successfully large scale ordering at low activity rates, and presence of inhomogeneities in the density of polar active matter in the form of bands. Similar analysis was used to justify experimentally observed number density fluctuations well above the equilibrium statistical mechanics prediction of $\langle N^2 \rangle \sim \sqrt{\langle N \rangle}$[19, 20]. Similar to the aforementioned cases of polar active matter, continuum equations for polar and nematic active matter in dry and wet systems have been formulated and used to predict stability of solutions [19].

As a consequence of having continuum equations for the dynamics of active matter system, modeling of active matter computationally through numerically solving these full non-linear equations has proven quite fruitful. One such model was created to model systems of active polar rods. It demonstrated that given densities above a critical value and self propulsion velocities below a critical value, the system of rods saw the persistent development and devolution of a multitude of flocks of different sizes. Further this study showed that above

a critical value of propulsion speed, while the density of rods is above a critical value, the rods formed thick bands which contain particles moving the same direction followed by disordered regions [22]. A second example of numerical solving of continuum active matter theory is illustrated by a recent model of an arbitrary dry active nematic system. This model solved for an arbitrary active nematic as, through toggling of the elastic and activity constants of the system, one can recover the simple polar Vicsek model, and previously studied continuum formulations of active nematics with it. Within this model initially nematically aligned states were found to be unstable if the splay energies of the nematic were larger than bend energies to a certain extent. This resulted in an undulating state which could remain stable, or devolve into a defect-filled state. Below the parameters of bending instability which cause undulation, high levels of active torque relative active convection results in defects developing and forming a dynamic polar ordered system. High levels of activity and bend instability resulted in a turbulent nematic state filled with defects [26].

2.2 Polar active matter on a sphere:

Within the framework of active matter it is possible to find out how a polar flock would move along the surface of a sphere. Active matter studies have predominantly been performed on squares with continuous boundary conditions, implicitly a torus. It is hard to imagine a situation in which active matter would be confined to this topology in real life. A sphere represents a better approximation of the shape of cells along which bacteria typically travel. Vicsek models can be easily added to a sphere, only requiring that motion at each time step not allow the particles to leave the surface of the sphere. Hydrodynamic theories of arbitrarily aligning active particles fixed to a 2D manifold has been

developed [10]. Consequently numerical solving of these continuum theories over a sphere could also be accomplished.

2.2.1 Established work:

Recently researchers placed a polar Vicsek model with soft repulsion on a sphere and observed the formation of a band. The Vicsek particles moved with constant velocity in the direction they were facing at the start of each iteration. If the particles were within a certain radius of one another, their directions aligned via ferromagnetic coupling as in an XY model. These particles were made to experience a finite magnitude, short-range repulsion which push the particles directly away from one another. Both these forces were constrained to linear order to be tangent the surface of the sphere. The chief results of study were that at low rates of self propulsion the particles spread evenly across the sphere, moving in the same direction except about the poles. At the poles there persisted particles which could not move in the mean direction while simultaneously maintaining their direction tangent the sphere [27]. This is an expected consequence of the fact that a sphere has a +2 topological charge, and thus any attempt to align lines parallel one another along it must result in a net of +2 singular points where these lines cannot be parallel. At high rates of self propulsion the particles compressed together and formed a defect-free band [27]. Fascinatingly this suggests that polar matter, even when confined to different topologies than a torus, attempt to undergo the same disorder to ordered, defect free, state transition.

These simulations probed the dynamics of bacteria densely packed onto a sphere incapable of sudden changes in density. The results presented focused on the case in which 3000 particles had a soft potential radius applied to a radius σ around them corresponding to a packing fraction of $\phi = 1$. As

ϕ signifies the fraction of area of the large sphere covered in soft particles, the active particles completely covered the sphere. The repulsive force was activated if the particles were within 2σ of one another. Further this band was observed when particle directions aligned at a distance of 2.4σ. The density was prevented from suddenly fluctuating via inclusion of a term μ, scaling the repulsive term such that given the length scale of the simulation τ and elasticity of the repulsion k that $\mu = \frac{1}{\tau k}$. As a result an active motion leading to particles centers of masses coming within σ of one another is made impossible at any given time step, ignoring even the presence of on average 3-4 neighbors in front of them. As a result large number density fluctuations are made exceedingly unlikely in this model.

2.2.2 New results exploring ouroboros phase:

2.2.2.1 Description of model used:

A model equivalent to the one detailed above was created to investigate the dynamics of banding on spheres, which will be referred to as the ouroboros phase. At each time step particles moved at a constant angular velocity ω in the direction of their orientation. These orientations updated when particles were within a radial active interaction radius of one another, known as ang_{act} and with an elasticity k_{act}. During each iteration for particle i within ang_{act} of particle j a direction update would be updated via $\vec{n}_{i_{n+1}} = M_{(i,j)_n}.\vec{n}_{i_n}$ via the rotation matrix $M_{(i,j)_n}$. The matrix $M_{(i,j)_n}$was assembled to be the rotation matrix which would rotate $\vec{n}_{i_n}$ by $k_{elast}(1 - \vec{n}_{i_n}.\vec{n}_{j_n})$ radians in the hyperplane spanned by $\vec{n}_{i_n}$and $\vec{n}_{j_n}$ towards $\vec{n}_{j_n}$. The particles were made soft by making all particles within ang_{soft} angular separation from one another, move a prescribed distance along a geodesic taking them away from one another as directly as possible. At each step for particle i within ang_{soft} of particle j the position $\vec{x}_{i_n}$

would be updated via moving it along the geodesic defined by the direction $\vec{x}_{i_n} - \vec{x}_{j_n}$the distance $k_{soft}(ang_{soft} - sep_{(i,j)})dt^2$ where $sep_{(i,j)}$ is the angular separation of $\vec{x}_{i_n}$ and $\vec{x}_{j_n}$. No noise was added in the direction of the particles.

Testing of this model aimed to elucidate how soft bacteria, or other flocking systems, spread across a sphere could form in actual physical systems. Though packing fraction $\phi = 1$ regimes are of interest, it is hard to imagine how so many active particles could be confined to a sphere. As a result packing fractions substantially below this limit were tested. Further a range of different elastic repulsion levels was tested in order to allow for Vicsek-like massive number density fluctuations to occur on the novel spherical topology. To this end simulations were started in random configurations of positions, and directions. They were then numerically integrated using Euler-integration for 70,000 iterations. This system reaches dynamic steady states which is not currently understood. Thus a more rigorous condition for having reached equilibrium than all particles having been integrated many times was not used.

2.2.2.2 Categorization of the ouroboros phase:

Before delving into more abstract analytical methods it is first helpful to view a few configurations of the Vicsek model. Two such figures are shown below for a system after 70,000 iterations of integration. Note that in order to make the parameters easier to contextualize, all angular quantities/arc length dependent quantities are given in terms of the radius of particles corresponding to packing fraction 1, σ. :

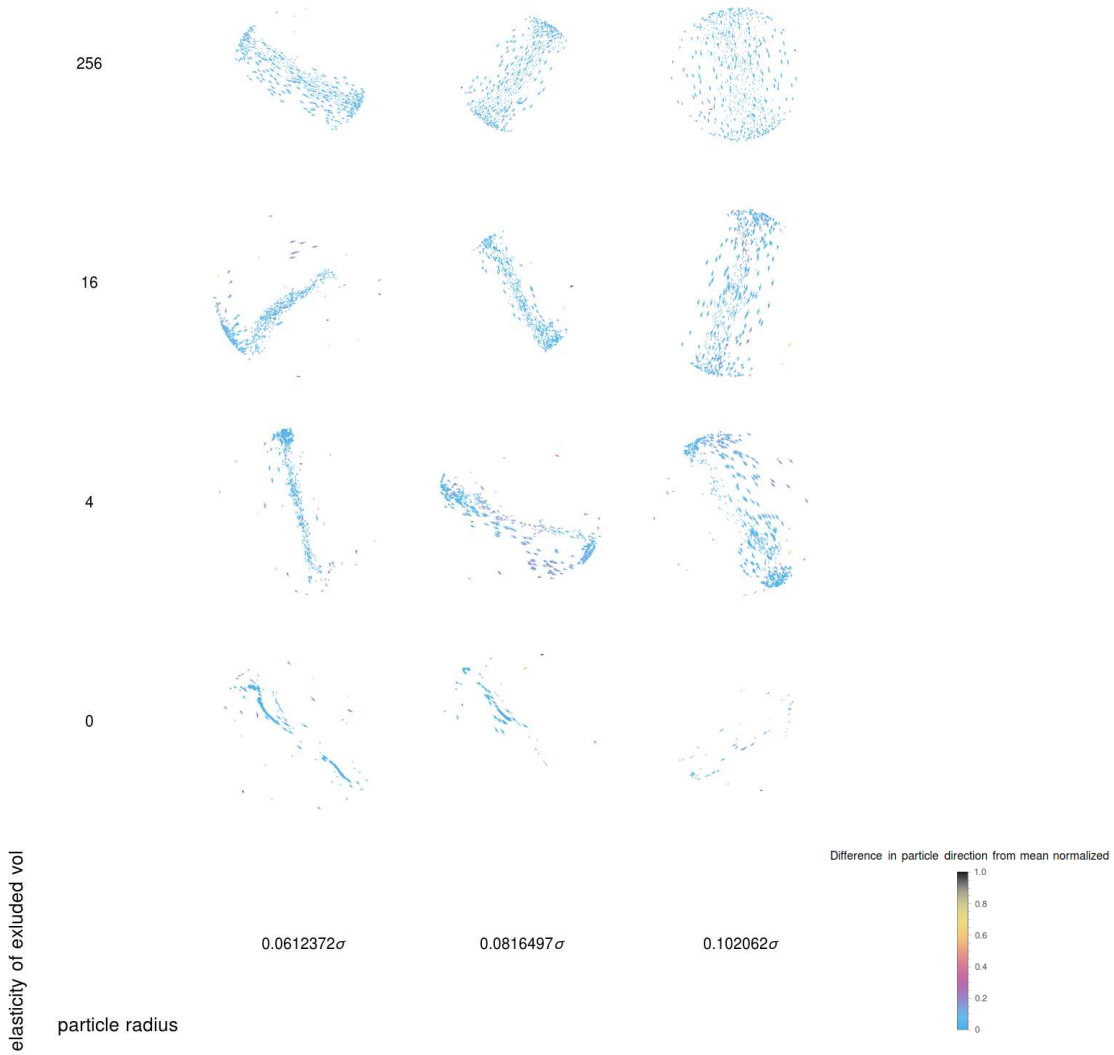

Figure 2.2.1: Active steady state for N=600, $\omega = \frac{6.4\sigma}{s}$, $ang_{act} = .77\sigma$ and $k_{act} = 0.05$ shows great circle ouroboros phase

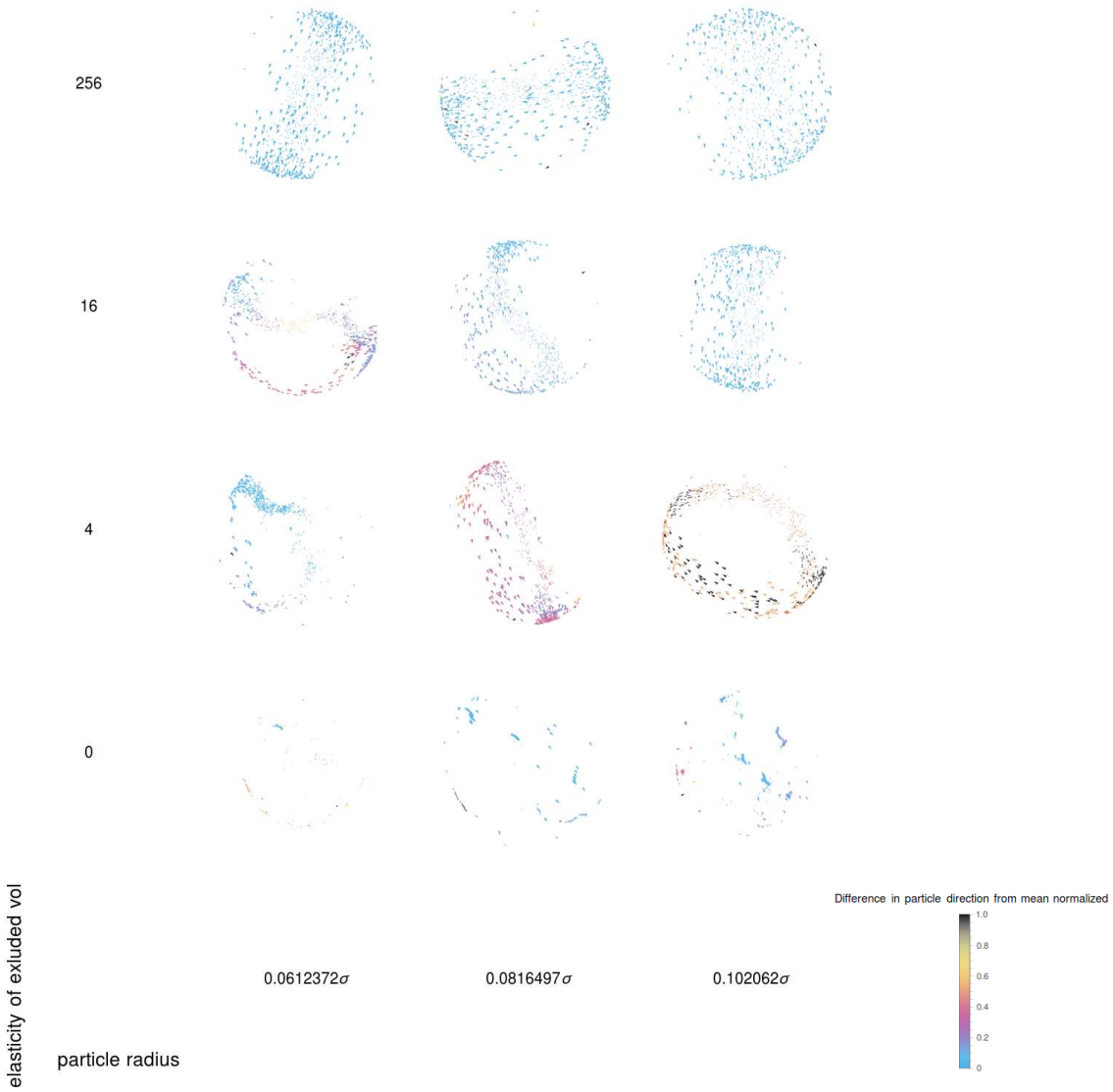

Figure 2.2.2: Active steady state for N=600, $\omega = \frac{3.2\sigma}{s}$, $ang_{act} = .77\sigma$ and $k_{act} = 0.05$ shows non-great circle ouroboros phase

These few frames show that at higher levels of activity the single uniform band previously seen develops. Given less activity the system tends to bend in novel ways previously not observed. However simply by viewing these frames it is hard to relate the available parameters, $\{N, \omega, ang_{act}, k_{act}, ang_{soft}, k_{soft}\}$ to the type of ouroboros phase which arises.

A convenient means to elucidate connection between these variables was to Fourier transform the positions of the particles after 70,000 iterations over a

sets of parameters. This would reveal which variables contribute to formation of small integer modes above $k = 1$, i.e. kinked ouroboros phases. Fourier transformation would demonstrate which parameters contribute to forming of turbulent states without visible modes. To this end the final frame from runs were collected for choice parameter values. These final frames have their final positions rotated such that the mean position cross direction value is at $\{0, 0, 1\}$. The position data was then converted into spherical coordinates θ and ϕ. The ϕ data is then Fourier transformed along the known interval θ.

Below the Fourier transform of active steady states over a range of different particles numbers which generated bands can be studied. A direct picture of the steady states of the 1000 particle case will be shown afterward each for reference.

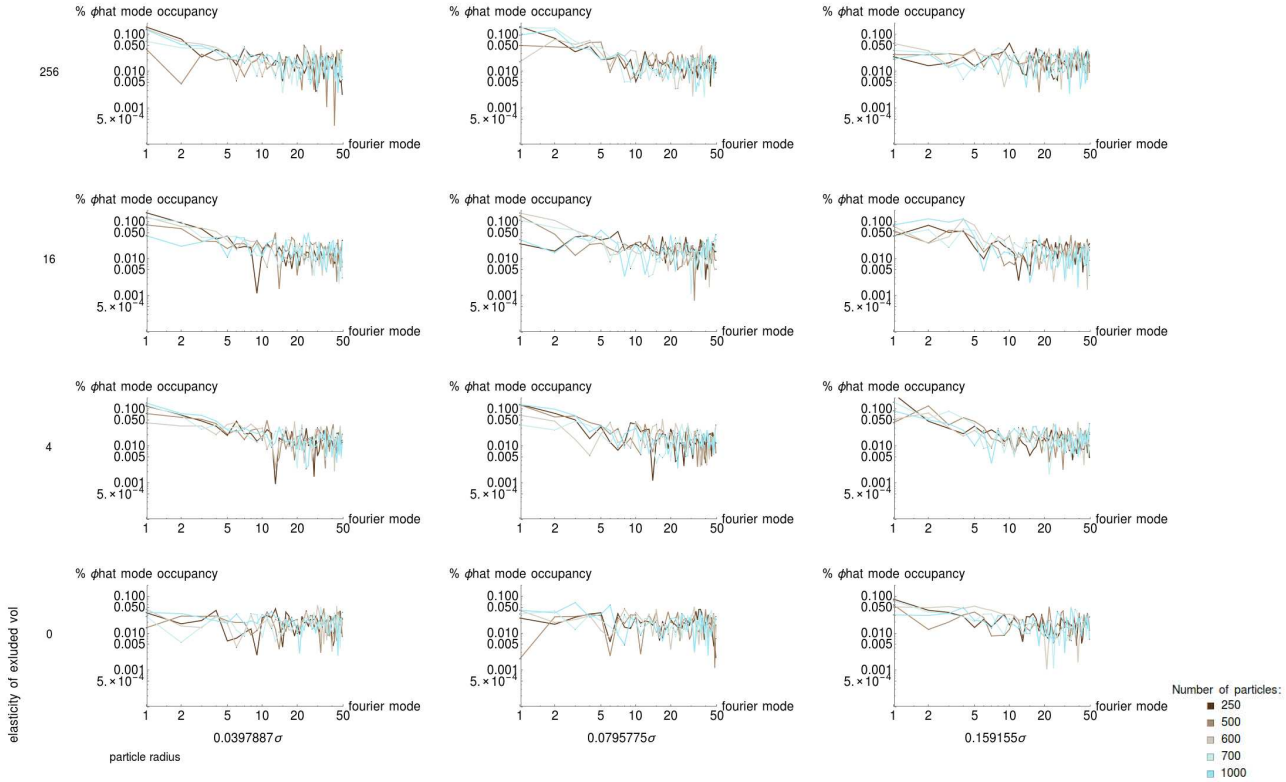

Figure 2.2.3: Fourier transform of active steady states of range of particle numbers for $\omega = \frac{4\sigma}{s}$, $ang_{act} = \frac{\sigma}{2}$ and $k_{act} = 0.1$

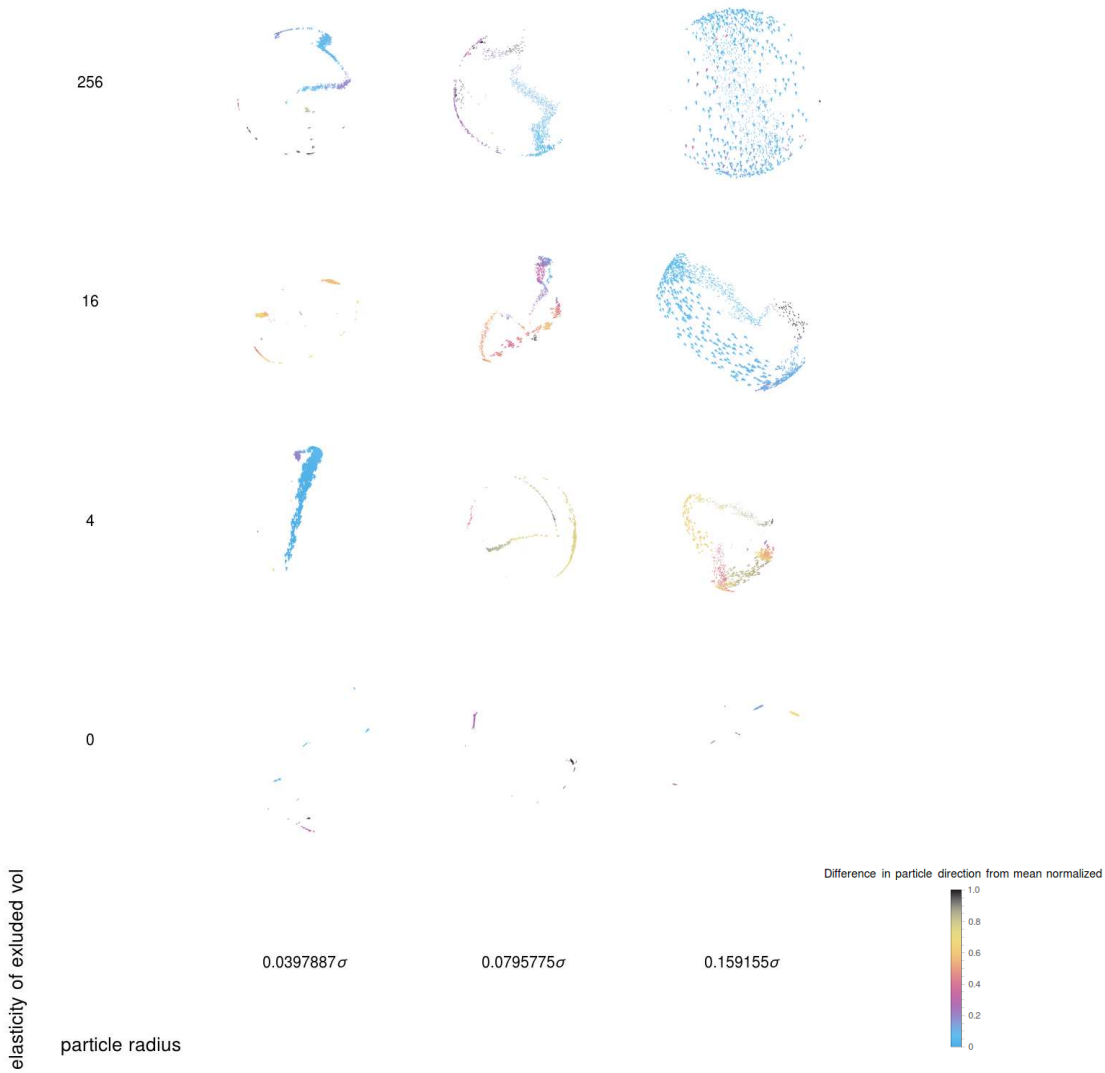

Figure 2.2.4: Active steady state for N=1000, $\omega = \frac{4\sigma}{s}$, $ang_{act} = \frac{\sigma}{2}$ and $k_{act} = 0.1$ to be Fourier transformed

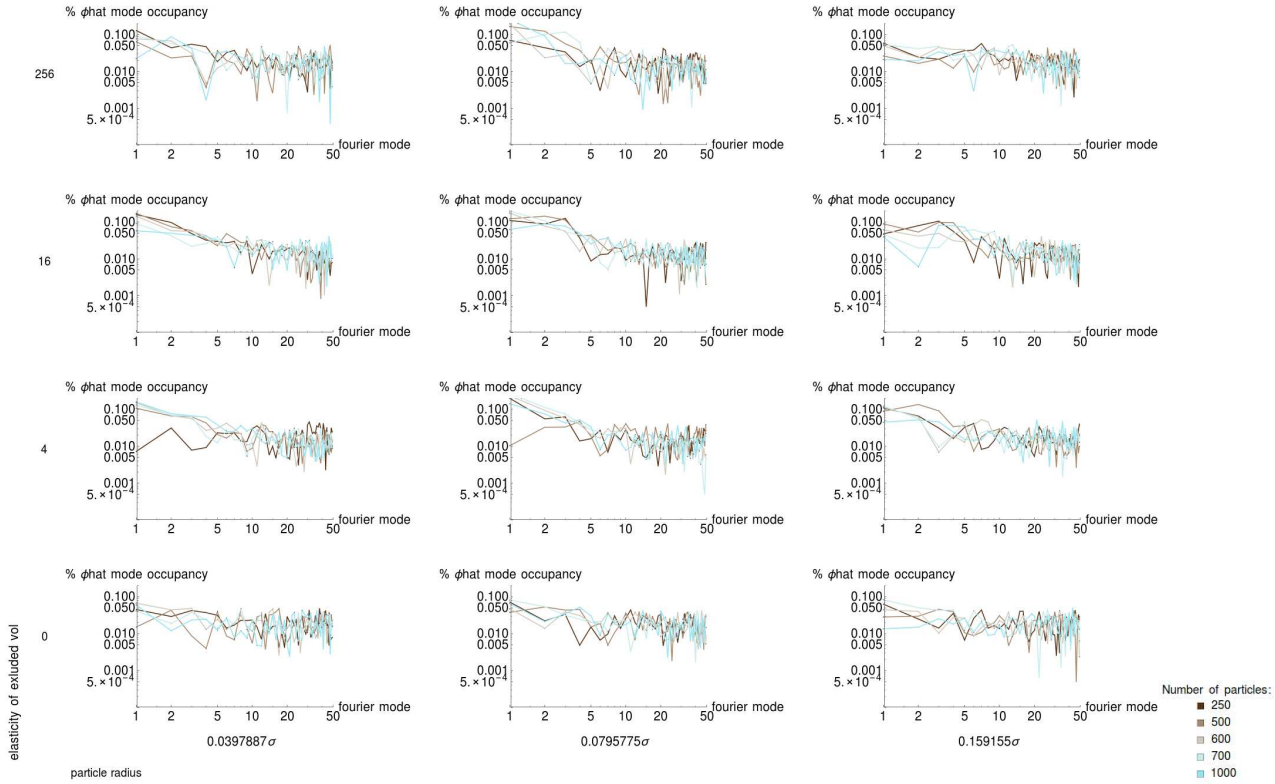

Figure 2.2.5: Fourier transform of active steady states of range of particle numbers for $\omega = \frac{4\sigma}{s}$, $ang_{act} = 2\sigma$ and $k_{act} = 0.1$

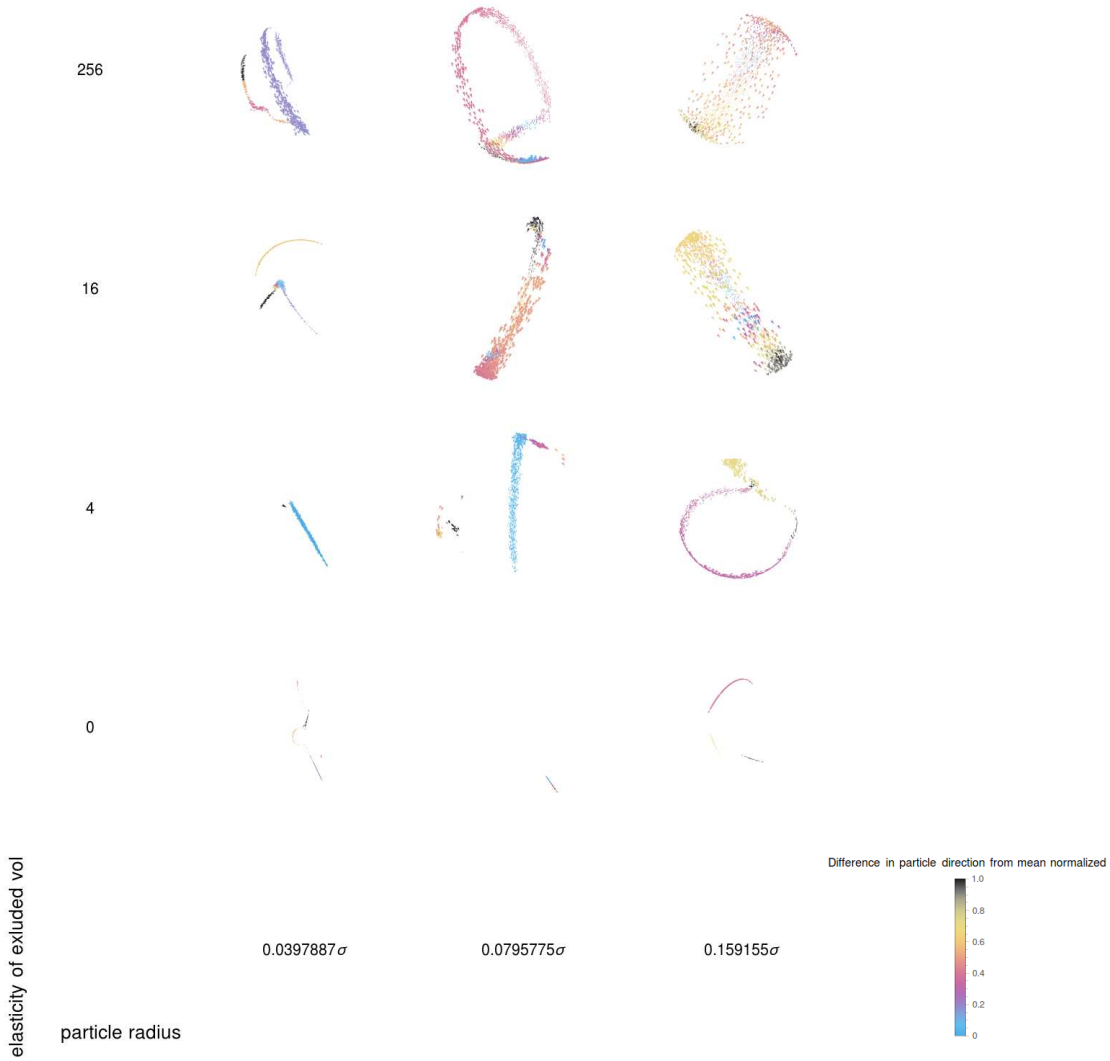

Figure 2.2.6: Active steady state for N=1000, $\omega = \frac{4\sigma}{s}$, $ang_{act} = 2\sigma$ and $k_{act} = 0.1$ to be Fourier transformed

Increasing the rigidity and radii of active polar particles causes the ouroboros phase to become kinked to the point that it becomes an indistinct band. All figures directly showing configurations of runs with no soft repulsion, i.e. when $k_{soft} = 0$, show linear flocks forming. These linear flocks do not form an ouroboros, instead generally forming many non-interacting linear flocks. The Fourier transforms about the mean direction of these flocks are noisy and uninformative as a result. The inclusion of repulsion for $k_{soft} \in \{4, 16\}$ results in the first few modes being significantly more likely to be occupied than

higher energy modes. This is due to the fact repulsion causes spreading across the surface of the sphere increasing their odds of joining a single ouroboros. Further for a given k_{soft}, increasing particle radius, ang_{soft}, pushes the peak of mode probability towards higher modes. The migration towards higher modes reflects that the ouroboros is becoming more self-repulsive and kinked to accommodate the energy of the particles repulsing one another over a long distance. Eventually, as shown by $k_{soft} = 256$ and $ang_{soft} = .159\sigma$, the repulsion has caused higher modes and lower modes to be equally likely. As can be seen in direct views of this state for 1000 particles, this forms a solid band.

Now Fourier transforms of the same parameter set over a range of different levels of activity will be shown:

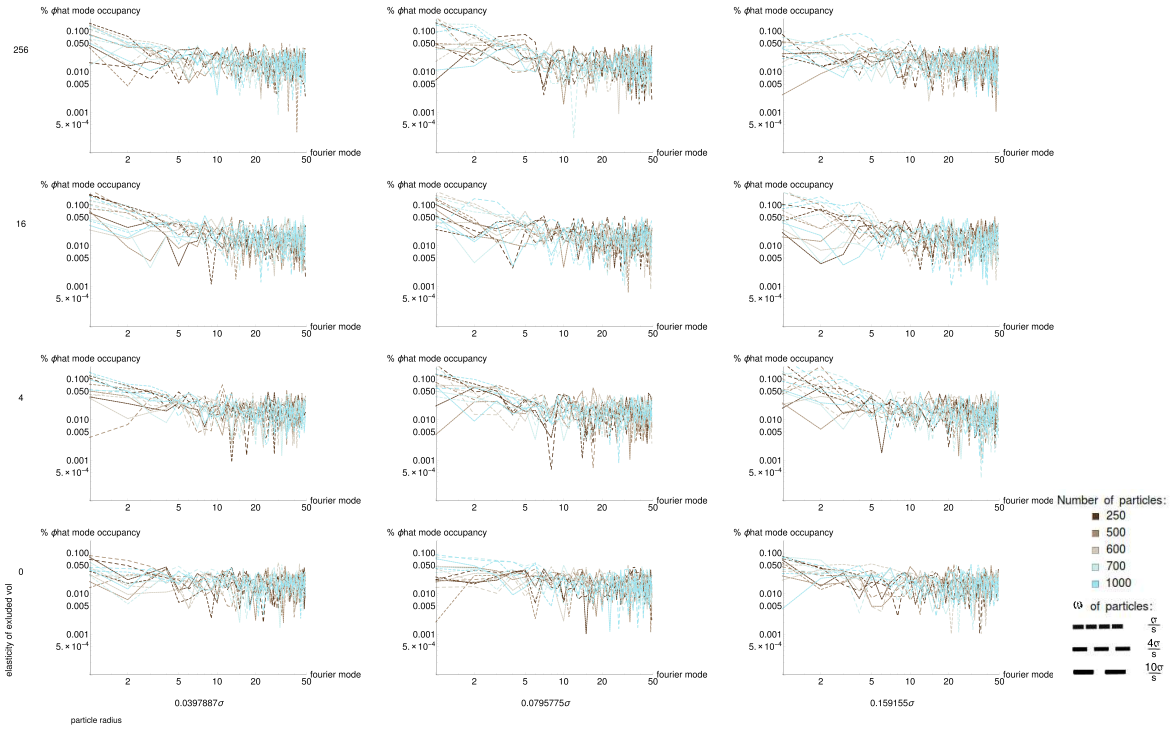

Figure 2.2.7: Fourier transform of active steady states of range of particle numbers and ω given $ang_{act} = \frac{\sigma}{2}$ and $k_{act} = 0.1$

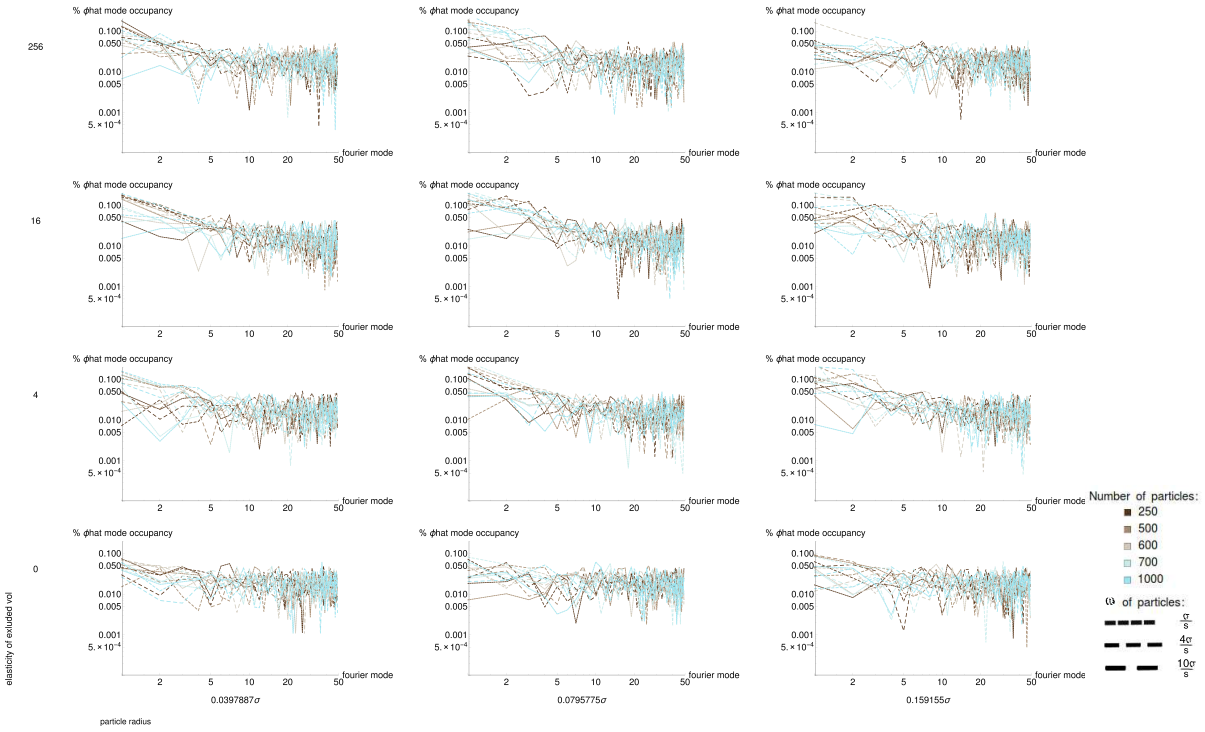

Figure 2.2.8: Fourier transform of active steady states of range of particle numbers and ω given $ang_{act} = 2\sigma$ and $k_{act} = 0.1$

Increases in angular momentum of the particles do not alter the trend of increasing active particle radii and rigidity driving the formation of progressively more kinked ouroboroses. Non-zero particle rigidity drives the formation of an ouroboros. For any given level of non-zero rigidity, increasing the radii of particles shifts the peak of the mode occupancy of the particles towards higher modes. Unfortunately as the data is quite noisy, it is hard to tell what role increasing angular momentum has on the dynamics of the system otherwise.

The chief conclusion that higher particle rigidity and radii drive the formation of bands is in agreement with past work. Past studies found, testing at high levels with large particles of radius equal to σ exclusively, only the formation of indistinct bands. Tracking of individual particles within this ouroboros revealed they were not moving along fixed great circles, but instead moving up and down within the band as they traveled as a part of it[27]. It has been revealed

that this motion is due to particles following sinusoidal paths about a great circle. At low densities of soft particles these paths can be exceedingly kinked and exotic. When they are large and rigid they act as in previous treatments; following a wide range of modes about the great circle in an indistinct band.

This model did not reveal a simple great circle phase as did the previous work, likely as it lacks noise. Other researchers reported that without any rigidity a Vicsek model on a sphere always forms a band about a great circle [27]. With this model however only disconnected linear segments of particles were found when the particles do not repel one another. Yet this difference is easily explained as this model does not contain noise. As a result once a grouping of particles polarize to move in the same direction, they will not stray from this path unless any of the members of the flock are within ang_{act} of another particle facing a different direction at any given time step. Multiple flocks along different trajectories will thus never meeting and form a single band. On the other hand within the previous model such groups, and free particles within the system, would explore the system due to the noise in their orientation at each step.

2.2.2.3 Future work:

The role of initial disorder in this system ought to be explored during future experimentation. The initially random directions and positions of the particles of this model may obscure the study of this system. Via starting from random starting conditions differing parameter valued trials were started invariably from states of differing levels of order. Future studies ought to start particles from controlled starting positions and orientations. Gradually introducing disorder to these quantities, rather than the soft and active components of the system, may reveal more tractable results.

A line of investigation which could be pursued with this model at minimal cost could be testing the impact of simple nematic alignment on the dynamics of the system. Changing the direction to which particles align based on their neighbors could be easily altered. For example instead of promoting alignment to the same direction as their neighbors, it would be just as easy to promote alignment in the opposite direction. Inclusion of a new parameter which controlled the radian degree of alignment away from the same as the direction as their neighbors could be easily included and batch tested. While this would not allow one to test how an arbitrary active nematic would align along the surface of a sphere, it would allow comparison to a wide variety of simple active nematics.

Chapter 3

Combining active mater and deformable surfaces:

In addition to relatively well understood categories of active matter in dry, and wet systems, active matter can be a constituent in gels which contain bulk elasticity. In fact the bulk of biological beings are composed of viscoelastic gels which are propelled by active constituents. For this reason this category of active matter systems has the potential to elucidate how biological beings, ensembles of soft yet solid particles, move as a result of chemical energy being introduced locally to specific active matter systems. Even more intriguing is the prospect of being able to assemble relatively stiff gelatinous systems yet which can be programmed into a range of different configurations. Clearly a subfield of this broad set of systems are those in which the active component of the system is limited to move along the surface of a gel, i.e. a deformable surface.

3.1 Established theoretical work:

In spite of the potential impact, and interest in understanding active matter in or on viscoelastic gels, there has been relatively little progress in developing a framework as robust as for dry and wet systems to describe them. In the case of active matter in wet and dry systems perturbations around equilibrium and linearizations yielded fruitful comparisons to experimental systems of interest and numerical simulations. On the other hand when active matter lies within gels perturbations around the gel in equilibrium simply does not produce models about experimentally interesting biological systems far from equilibrium. A typical assumption during this work is that a given viscoelastic gel is a Maxwell material relaxes from deflected states decay on a single relaxation time, i.e. proportional to $\exp(-\frac{t}{\tau})$ where $\frac{d\tau}{dt} = 0$ [19]. Large deformations of cells have to the contrary a wide range of different dissipation times. Arguing that there must be a distribution of relaxation times at work in cell deformation processes, relaxation via a distribution of different power laws [2]. Simply stated, the lack of a generalized framework for describing soft solids, viscoelastic gels, has proved the limiting reagent in the description of active matter on deformable surfaces and in deformable bulks.

Lacking firm theoretical predictions out of equilibrium in non-linear regions, numerical solving of the continuum equations have served to give insight into the behavior of active viscoelastic gels. An example of one such model is lattice Boltzmann model of active liquid crystals subject to external flow. This simulator allowed the evolution of a system obeying an Beris-Edwards description of liquid crystal hydrodynamics however with an additional activity term within its stress tensor. The activity term was a real valued scaled form of the liquid crystals tensor order parameter. As a result this activity can promote ordering or tumbling. It was found that order promoting activity, in LCs known

as extensile or aligning, activity initially increased the velocity of the flow of the LC yet converged to the passive LC flow rate. Contractile active LCs, whose activity penalize alignment, chiefly exhibit an 100-fold increase in viscosity over inactive LCs of the same type [1]. Such models succeeded in elucidating the non-linear regimes of activity in active viscoelastics beyond theoretical models and actor models. Yet examples of the use of similar techniques to probe the dynamics of active particles interacting with a deformable surface remain elusive.

3.2 Established experimental work:

Experimental exploration of coupled deformable surfaces and active matter has exhibited fascinating periodic defect motion, and cilia formation. Said study was based upon observation of an active nematic system placed on a lipid vesicle. The active nematic system was composed of microtubules, elastic rods, being propelled by pairs of kinesin motor proteins bound together. The volume excluding polymer PEG was added to these lipids to force the microtubules, and motor protein bundles to lay along the surface of the lipid and cluster together. The ATP consuming motor protein bundles persistently prevented the microtubules from forming a relaxed liquid crystal phase along the surface. As a result what was observed were liquid crystal phases with two +1 defects or four $+\frac{1}{2}$ defects, minimizing the elasticity of the microtubules subject to the frustrating Gaussian curvature of the spherical vesicle [17]. Vesicles formed out of passive nematic liquid crystals forced to anchor tangentially both the inner and outer water form between 2, 3, or 4 defects which always add up to a +2 topological charge via combinations of exclusively +1 and $+\frac{1}{2}$ charges [18]. While intriguing that within the active vesicle system 3 defects never

persisted, it is clear that the microtubules were being perturbed away from a near equilibrium liquid crystal configuration. When 4 defects were present they oscillated between a tetrahedral and planar configuration with a frequency closely related to the amount of ATP, i.e. activity, in the system. Further when vesicles covered in 4 defects had their volumes shrunk, 4 exceedingly fine cilia-like structures protruded from the lipid and rotated about it over hours [17].

Though this system was created as a minimal model of biological surfaces interacting with active matter, there are a number of distinct types of dynamics likely at play. Firstly there is an active nematic system of microtubules and kinesin bundles. There exist a wealth of microscopic and phenomenological actor models, and continuum models of these systems explicitly discussed in section:2.1, section:3.1 , and featured in the review [19]. Further the dynamics of the lipid vesicle are necessary for a full description. Clearly in cases in which the lipid vesicle is highly deformed the elastic response of the lipid vesicle is at play. In these highly deformed regimes the elastic response will not be well-approximated by a linearized elastic theory. Also cilia formation did not result just from the vesicles force response, and the activity of the active nematic, but through shrinking the volume of the vesicle [17]. Lipid budding, when not due to changes in lipid composition of the vesicle, has been experimentally shown to occur most prominently when the vesicle in question formed leaks [13]. Thus cilia formation is may be tied to the poorly understood problem of lipid budding.

3.3 Modeling active matter on deformable surfaces:

Having a wide range of different models of active matter, and no clear consensus on how to model deformable surfaces, it is not immediately clear which to use to construct a generalized framework to model active matter coupled to deformable surfaces. The main result from the work performed thus far with active matter has been that for any given class of active matter one desires to model, careful construction of relevant actor models and continuum equations can replicate experimental results. The original work presented in chapter 1 has shown that numerical minimization of carefully chosen energy functionals has promise for modeling arbitrary deformable surfaces. Consequently it is recommended that future researchers model active matter on deformable surfaces through numerical minimization of energy functionals along surface representative meshes with carefully chosen active matter models placed on them or included through adding their energies directly into the minimization of the mesh.

As concluded in chapter 1 the dynamics of numerical minimization ought to be carefully compared to experiments before proceeding to model active systems in the vast majority of cases in which active matter components of the system of interest work do not operate on time-scales far slower than the surface. The static behavior of energy minimal models of liquids and soft solids has been shown to be in excellent agreement experiments. Thus if active matter on a deformable surfaces moves far slower than the surface, the system could be physically modeled through alternating between numerically projecting the active matter system forward in time, and relaxing the mesh in response until it reaches a strict equilibrium condition. However in the vast majority

of cases of interest active matter moves relatively quickly. In such cases the active and deformable systems need to be relaxed as closely to at the same time as numerically possible. Thus it is essential that a numerical action or energy minimization technique be selected that can be integrated by known physical length scales. Such a known change in length scale would allow the active system to be relaxed in similar steps, allowing the processes to evolve side-by-side physically.

A possible method for modeling diffuse or strongly topologically confined active matter would involve directly moving actor models across a deformable surface mesh. Currently Morpho has the capacity to return the point along a mesh which is a given distance along its geodesic started from a given starting point and direction. This provides a means by which active particles can be moved along an arbitrary mesh. This routine however is computationally expensive as it must iteratively trace the path along the mesh to find the end point. Pending development of a drastically improved geodesic tracing function, only less than 100 particles should be moved across a given mesh at a time. However experimental active matter deformable surface systems may be well modeled by only a handful of particles. In the case of the Keber experiment, a successful model of the oscillating 4 defect phase was accomplished through numerical integration of the 4 defects [17]. Though in many cases the number of defects in active systems vary, in the cases in which they do not, due to topological confinement or otherwise, there exists promise that modeling just their motions describe the motion of the active matter. Clearly a system containing only a few active matter particles could be modeled directly using this technique regardless of topology.

Given the success of continuum active matter models another option available is to place film-like continuum models on top of deformable meshes. In the

limit of a system containing many active particles per surface area, a continuum model of active matter is most appropriate. A continuum theory could be numerically projected forward in time on a grid defined along the surface of the mesh on the same time scale as the deformable surface is evolved. This continuum theory would have to account for the fact that active system is film-like as well as along a curved surface. Dr. Marchetti has already proposed that film-like active matter systems ought to have strict anchoring conditions along the surface they travel along, and possess an incompressibility condition reflecting conservation of volume of the film [19]. Further continuum theories of polar active matter confined along curved surfaces have already been created [10]. For a given mesh, local curvatures about regions of active matter required for these equations could be estimated to varying degrees of accuracy proportional on the refinement of the mesh. One technical complication with this technique would be the fact that the surface discretization would change during simulations, necessitating changes of the discretization of the continuum solution. As a result finite element solutions to these continuum solutions, which easily allow for non-uniform discretization of solutions, would be required rather than the common finite difference schemes used currently.

A final, albeit experimental, possible solution is the direct minimization of active matter and surface free energies. The hydrodynamic equations which are numerically solved for in active matter studies are based upon arguments about the free energy of the system. As a result minimizing the formulations of the action of these free energies ought to replicate the dynamics of the system. Consequently the solving of active matter system motion via action minimization could be placed directly into the framework as the surface. Active matter theorists have already developed Landau-de Gennes expressions for the free energy of active nematic systems [30]. Theoretically with both active and

deformable components of a system of interest combined in an action minimal framework one could prevent the motion of one component from accidentally entering a configuration which is highly energetically unfavorable for the other.

Chapter 4

Appendix:

4.1 Proof of catenoidal solution to area minimal deflected disk:

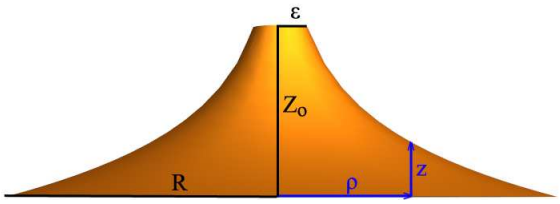

Figure 4.1.1: Parametrization of deflected area minimal disk

4.1.0.4 Monge parametrization of the surface:

$$\vec{x} = \begin{bmatrix} \rho\cos\theta \\ \rho\sin\theta \\ \alpha z(\rho) \end{bmatrix} \tag{4.1.1}$$

4.1.0.5 Calculation of the coefficients of first fundamental form:

First we find the arbitrary form of any tangent along surface $\vec{x}$. Note that as no partial derivatives z of θ exist in the solution. Now let $z' \equiv \frac{\partial z(\rho)}{\partial \rho}$ and

$z'' \equiv \frac{\partial^2 z(\rho)}{\partial \rho^2}$.

$$\partial\rho = \frac{\partial}{\partial\rho}\vec{x} = \begin{bmatrix} \cos\theta \\ \sin\theta \\ \alpha \cdot z' \end{bmatrix}$$

$$\partial\theta = \frac{\partial}{\partial\theta}\vec{x} = \begin{bmatrix} -\rho\sin\theta \\ \rho\cos\theta \\ 0 \end{bmatrix}$$

Knowing this the coefficients of the first fundamental form are:

$$E = \partial\rho.\partial\rho = 1 + \alpha^2 z'^2$$

$$F = \partial\rho.\partial\theta = 0$$

$$G = \partial\theta.\partial\theta = \rho^2$$

$$A = \sqrt{EG - F^2} = \rho\sqrt{1 + \alpha^2 z'^2} \tag{4.1.2}$$

4.1.0.6 Creation of Euler-Lagrange equation to find stable solutions:

$$\frac{dL}{dz} - \frac{dL}{dz'} = -\frac{\alpha^2(z' + \alpha^2 z'^3 + \rho z'')}{(1 + \alpha^2 z'^2)^{\frac{3}{2}}} = 0 \tag{4.1.3}$$

4.1.0.7 Expansion of Euler-Lagrange equation about $\alpha = 0$:

$$(-z' - \rho z'')\alpha^2 + (z'^3 + 3\rho z'^2 z'')\frac{\alpha^4}{2} + O(\alpha)^5 = 0$$

4.1.0.8 Solving linear term of Euler-Lagrange equation expansion about $\alpha = 0$:

Laplace's equation for $z(\rho) \Longleftrightarrow$first expansion term

$$\nabla^2 z = 0 = \frac{\partial^2 z}{\partial \rho^2} + \frac{1}{\rho}\frac{\partial z}{\partial \rho} = \frac{z'}{\rho} + z'' \Longleftrightarrow 0 = -(z' + \rho z'')$$

Ansatz solution for Laplace equation

$$z(\rho) = C \cdot \ln \rho + D$$

Impose boundary conditions to Ansatz solution

$$z(R) = 0 \Rightarrow D = -C \ln R \; z(\epsilon) = z_o \Rightarrow z_o = C \ln(\frac{\epsilon}{R})$$

Leading to the solution

$$\text{zlinear}(\rho) = \begin{cases} \rho \leq \epsilon & z_o \\ \rho > \epsilon & \frac{z_o}{\ln(\epsilon/R)} \ln(\rho/R) \end{cases} \tag{4.1.4}$$

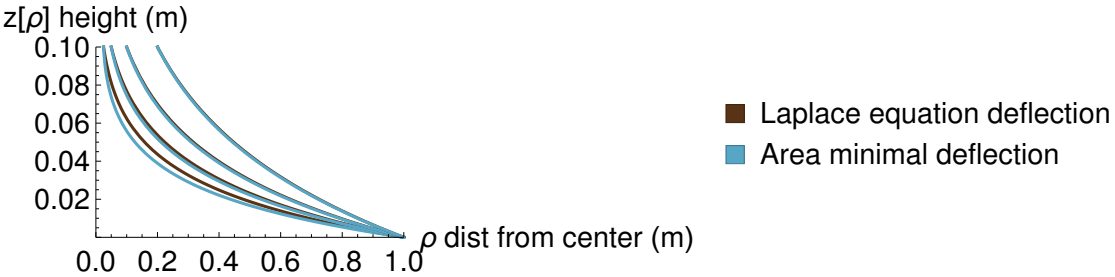

Figure 4.1.2: The linearized/Laplace's solution clearly begins to fail as an approximation as the width of deflections decrease

4.1.0.9 Discovery of full catenoidal solution:

Based on the observation that the z_{linear} appeared catenoidal, the solution of a catenoid in terms of ρ was plugged into the Euler-Lagrange equation 4.1.3. We found that it satisfied the Euler-Lagrange equation and thus concluded the all static deformations must obey the following equation of a catenoid:

$$z_{catenoid}(\rho) = b - a \cdot \text{arccosh}(\rho/a)$$

4.1.0.10 Imposing boundary conditions on catenoidal solution:

For the sake of mathematical brevity let us define z as:

$$\text{z}(\rho) \equiv z_{catenoid}(\rho)$$

As the catenoid must have a height of 0 at the edge of the disk

$$\text{z}(R) = 0 = b - a \cdot \text{arccosh}(\rho/a) \rightarrow b = \text{arccosh}(R/a) \tag{4.1.5}$$

As the catenoid must have height z_o at the edge of the inner raised disk

$$\text{z}(\epsilon) = z_o = b - a \cdot \text{arccosh}(\epsilon/a) \tag{4.1.6}$$

$$z_o = a \cdot \text{arccosh}(R/a) - \text{arccosh}(\epsilon/a) \tag{4.1.7}$$

This expression is maximized when $\text{arccosh}(\epsilon/a) = 0 \,|\epsilon = a$ thus:

$$z_{max} = \epsilon \cdot \text{arccosh}(R/\epsilon) \tag{4.1.8}$$

4.2 Forced droplet model:

One method attempted to test whether direct energy minimization resulted in structures with quantifiable elasticity was the creation of a 2d model of a droplet. This two dimensional model considered a droplet as a discrete loop which minimized line tension with an area energy constraint. By applying forces to this model it was suspected that the elastic modulus of the loop could be determined. This would solely be a matter of measuring the extent to which the loop deformed before reaching a new shape subject to a given force.

Unfortunately this model did not end up serving this end as testing of it was ended prematurely. After a month of focusing on this model, Dr. Jensen's experiments came to light. As the elastic modulus of water droplets is still not well studied, it was abandoned.

In spite of this, the model does illustrate how direct enforcement of constraints can prove problematic. Constraints within this model are enforced just as in Morpho. If on a given step via gradient descent the path to be taken to minimize the specified energies of interest at a given vertex are $\vec{F}$ and the constraints $\vec{C}$ then the applied path will be $\vec{F} - \frac{\vec{F}\cdot\vec{C}}{\vec{C}\cdot\vec{C}}\vec{C}$. Below are shown the paths to be taken via the next minimization step for minimizing line tension, area, and line tension constrained to not change area of discretized ellipses and circles.

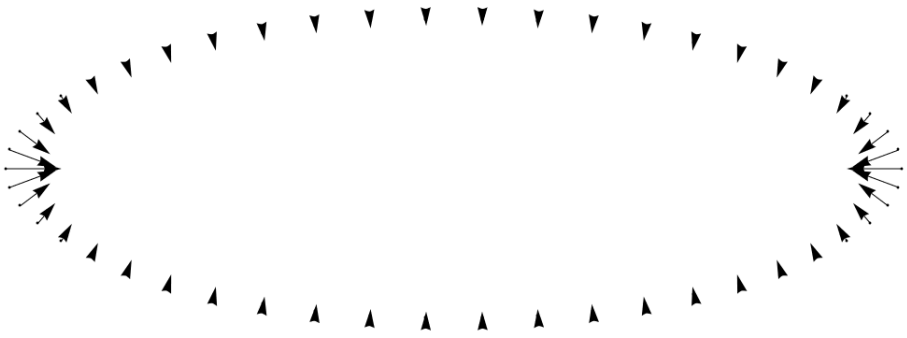

Figure 4.2.1: Direction of step of line tension minimization

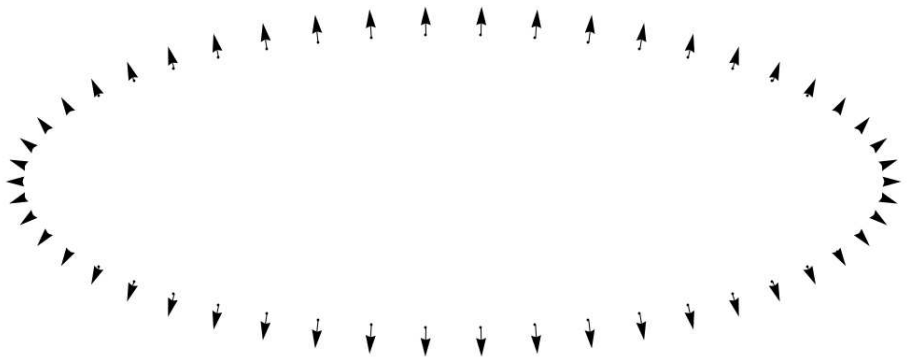

Figure 4.2.2: Direction of step of area maximization

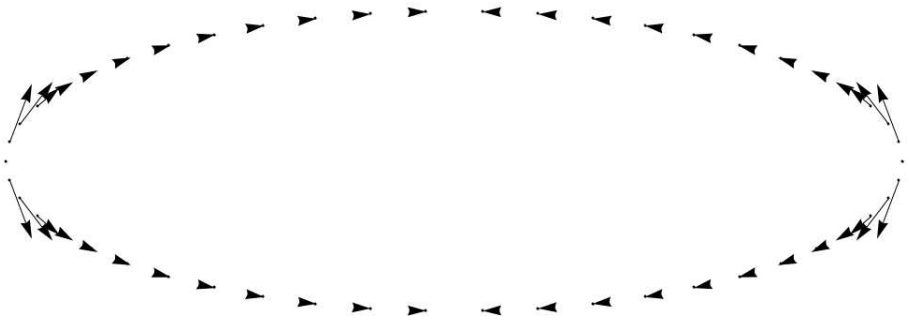

Figure 4.2.3: Direction of step of hard area constrained line tension relaxation

Overall in the case of an initially ellipsoidal droplet, energy minimization seems to guide the droplet towards a circular configuration. The points along the high curvature end points appear to be causing the area enclosed by the points to expand slightly. Simultaneously points are receding along the edge of the ellipse towards the center.

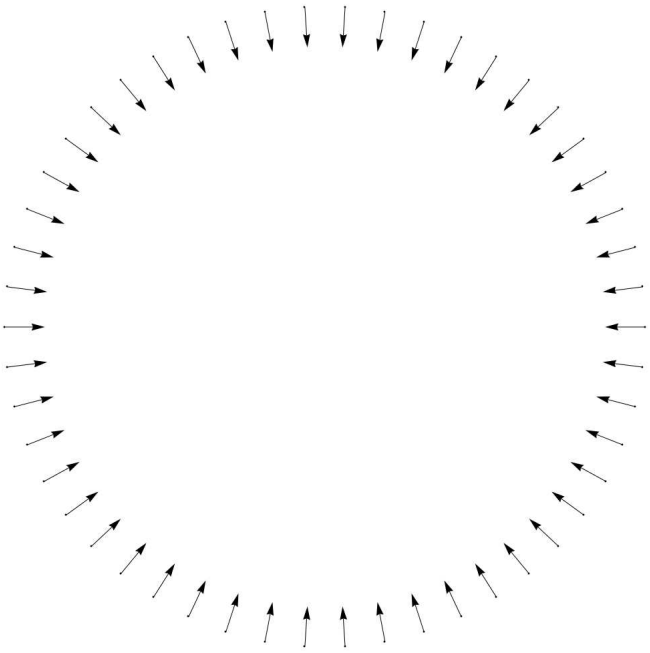

Figure 4.2.4: Direction of step of line tension minimization

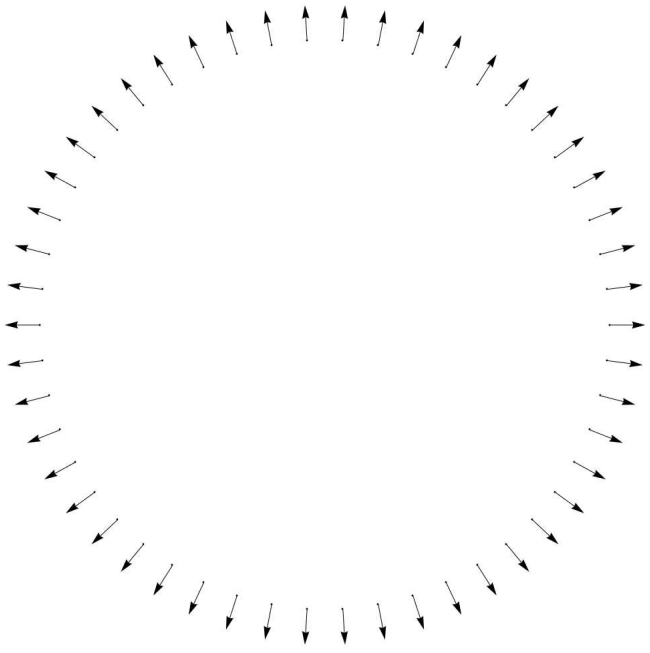

Figure 4.2.5: Direction of step of area maximization

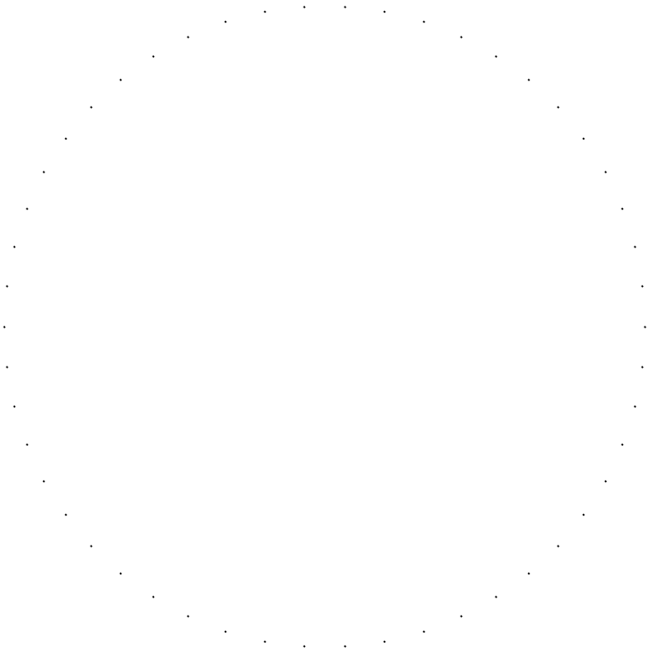

Figure 4.2.6: Direction of step of hard area constrained line tension relaxation

Similarly this relaxation scheme correctly reproduces the fact that the 2D shape with maximal length to area enclosed is a circle. When already placed in a circular configuration, the droplet's area and line tension energies perfectly balance out. As a result the droplet's points are not moved at all when asked to minimize line tension subject to an area constraint.

We will now consider an initially circular hard area constrained line tension minimal surface experiencing a Gaussian "force" per step. It is worth noting that this corresponds to having added an energy to the system whose negative gradient forms a Gaussian distribution.

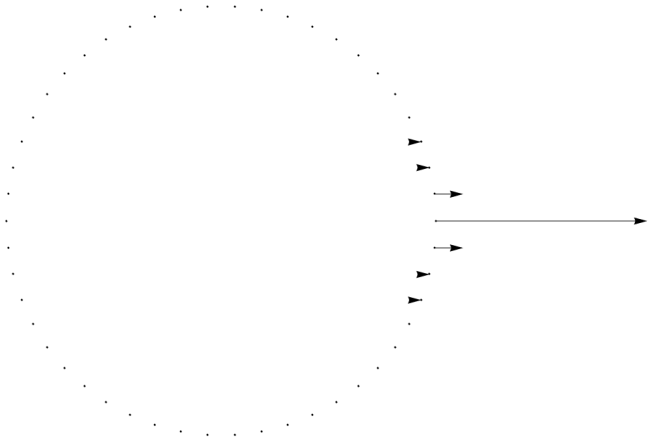

Figure 4.2.7: Direction of step of area constrained line tension and unconstrained Gaussian minimization

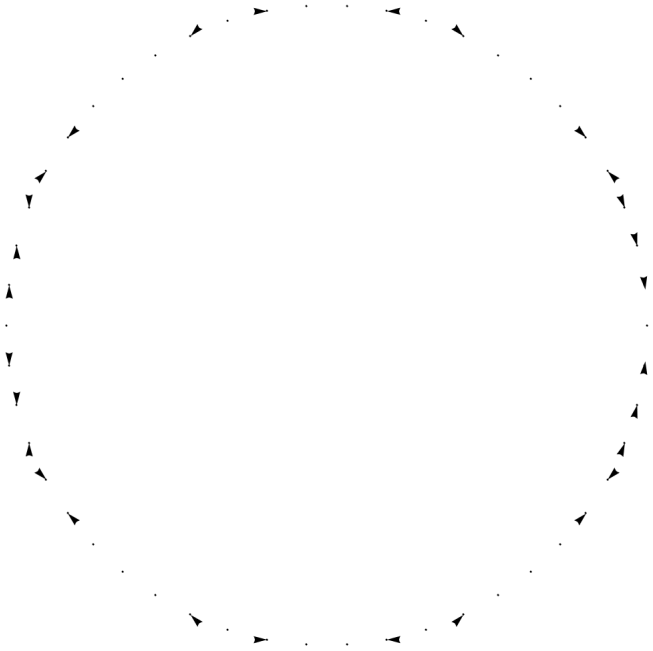

Figure 4.2.8: Direction of step of area constrained line tension and Gaussian minimization

It is clear here that the hard constraint scheme is problematic in the case

of an initially circular loop. This is due to the fact that the shape is already area minimal. Any step away from this configuration will increase area energy. Though the linear scheme of enforcing the area constraint completely will fail to remove the non-linear portions of the applied Gaussian and motion will occur, this does illustrate the problematic nature of trying to take a form out of equilibrium which has a hard constraint.

Knowing that enforcing hard constraints can prevent Morpho-like energy minimization from being deflected out of equilibrium, there do exist ways of simulating a departure from equilibrium with minimal changes to the algorithm. Firstly with no changes to the system one could simulate forces which are applied briefly over a time scale much faster than the relaxation of the body. This could be done by introducing an energy representing the force to the system, with no constraints or other energies active, and relax the system for the short period of time desired. The applied potential could be removed while other energies and constraints would be turned on. The mesh could then evolve in response to the applied potential. A more complicated approach would be to elastically enforce constrained quantities through using of conditional minimization and maximization of the constrained quantity. In the case of the droplet model we could remove the hard area constraint and given a desired conserved area A_{const} if at the n^{th} step the are was $|\vec{A}_n| < A_{const}$ perform a maximization step, i.e. given $\vec{F}$ is the sum of other gradients of energies being minimized perform the step $\vec{x}_{n+1} = \vec{x}_n - \lambda_f \vec{F}_n + \lambda_a \nabla \cdot \vec{A}_n$. Alternately if $|\vec{A}_n| > A_{const}$ a minimization step could be taken $\vec{x}_{n+1} = \vec{x}_n - \lambda_f \vec{F}_n - \lambda_a \nabla \cdot \vec{A}_n$.

4.3 Two dimensional Euler-Lagrange minimization of energy functionals:

4.3.0.11 Motivation:

After learning of the experimental dynamic soft solid and liquid relaxation behavior performed by Dr. Jensen, it was speculated that a simple two dimensional Euler-Lagrance formulation of energies would replicate her results better than Morpho. Though Dr. Jensen's results do not show rippling, indicating that momentum was not a large factor in the motion of the system, it is still uncertain whether or not minimizing the area and mean squared energies of the system, rather than an Euler-Lagrange formulation of them, would yield correct dynamic behavior. Further Dr. Jensen's results concerned relaxation of catenoidal structures, parametrized by a solution deflection $z(\rho)$, a function of ρ position along a radius which is implicitly rotated 360^{o}. Thus it was deemed unnecessary that models of this phenomena have 3 dimensions.

4.3.0.12 Details of model:

To this end a 2 dimensional model which could minimize the Euler-Lagrange formulation of an arbitrary ordinary differential equation along a line. Andrew DeBenedictis created a Mathematica notebook prototype which accepted a functional which depends solely on up to 2nd derivatives of deflection $z(\rho)$, a function of ρ position along a line, and ρ. Andrew's model minimized this function via steepest gradient descent with a constant length scale performed on the functional discretized using an first order accurate finite difference scheme. This was further improved by Ian who corrected mistakes in formulation of curvature energies, altered the discretization of the Euler-Lagrange form to be accurate to fourth order, sped up the code using matrices, added adaptive

length scale selection, and created Mathematica scripts out of it which could be batch tested on the Tufts computing cluster.

Euler-Lagrange formulation of area and mean squared curvature energies on disk: Using the Monge parametrization detailed in 4.1 we need only also calculate the coefficients of second fundamental form of the surface to obtain the mean curvature of the deflected disk:

First the ways in which tangent vectors along surface $\vec{x}$ can be varied must be calculated. Note that as no partial derivatives z of θ exist in the solution, $z' \equiv \frac{\partial z(\rho)}{\partial \rho}$ and $z'' \equiv \frac{\partial^2 z(\rho)}{\partial \rho^2}$:

$$\partial^2 \rho = \frac{\partial^2}{\partial \rho^2}\vec{x} = \alpha \begin{bmatrix} 0 \\ 0 \\ z'' \end{bmatrix}$$

$$\partial\rho\partial\theta = \frac{\partial}{\partial\rho}\frac{\partial}{\partial\theta}\vec{x} = \begin{bmatrix} -\sin(\theta) \\ \cos(\theta) \\ 0 \end{bmatrix}$$

$$\partial^2 \theta = \frac{\partial^2}{\partial \theta^2}\vec{x} = -\rho \begin{bmatrix} \cos(\theta) \\ \sin(\theta) \\ 0 \end{bmatrix}$$

Then the form of local perpendiculars form along $\vec{x}$ must be found using the tangents along $\vec{x}$ $\partial\rho$ and $\partial\theta$ calculated here4.1.0.5. :

$$\hat{n} = \frac{\partial\rho \times \partial\theta}{||\partial\rho \times \partial\theta||} = \frac{\rho}{\sqrt{\rho^2 + \alpha^2\rho^2 z'^2}} \begin{bmatrix} -\alpha\cos(\theta)z' \\ -\alpha\sin(\theta)z' \\ \rho \end{bmatrix}$$

Now the coefficients of the second fundamental form are:

$$e = \hat{n}.\partial^2\rho = \frac{\alpha z''}{\sqrt{1+\alpha^2 z'^2}}$$

$$f = \hat{n}.\partial\rho\partial\theta = 0$$

$$g = \hat{n}.\partial^2\theta = \frac{\alpha\rho^2 z'}{\sqrt{\rho^2(1+\alpha^2 z'^2)}}$$

Now the mean curvature of $\vec{x}\, H$ can be calculated as it solely depends on the coefficients of the first 2 fundamental forms:

$$H = \frac{eG - 2fF - gE}{2(EG - F^2)} = \frac{\alpha(z' + \alpha^2 z'^3 + \rho z'')}{2\rho(1+\alpha^2 z'^2)^{\frac{3}{2}}}$$

We also know that the Euler-Lagrange formulation for an energy functional $E(z(\rho))$ has second derivatives terms of z is of the form:

$$\frac{\partial E}{\partial z} - \frac{\partial}{\partial \rho}\frac{\partial E}{\partial z'} + \frac{\partial^2}{\partial \rho^2}\frac{\partial E}{z''} = 0$$

Thus Letting $E = H^2 + A$ yields the solution:

$$-\frac{2z'}{\sqrt{\alpha^2 z'^2+1}} + \frac{24\alpha^2 z'^3}{(\alpha^2 z'^2+1)^5} - \frac{2\rho z''}{(\alpha^2 z'^2+1)^{3/2}} + \frac{2z'+3\rho^2\left(z^{(3)}-\rho z''(\rho)\right)}{\rho^3(\alpha^2 z'^2+1)^2}$$
$$+\frac{3\alpha^2 z''\left(z'\left(2\rho z^{(3)}-2\left(\rho^2-4\right)z''\right)-7\rho z''^2\right)}{\rho(\alpha^2 z'^2+1)^4} + \frac{\left(\rho^2-4\right)z^{(3)}+5\rho z''-12\alpha^2 z' z''^2}{\rho(\alpha^2 z'^2+1)^3} = 0$$

In practice this expression was always linearized to first order about ρ before being minimized due to the complexity of established modeling techniques discretization it.

Letting $E = A$ yields the solution $-\frac{\alpha^2(z'+\alpha^2 z'^3+\rho z'')}{(1+\alpha^2 z'^2)^{\frac{3}{2}}} = 0$ as shown here 4.1.3.

4.3.0.13 Model demonstrates more plausible liquid dynamic behavior than Morpho:

In order to test how similar the relaxation of pure energy minimization performed by Morpho compared to relaxation of Euler-Lagrange formulations of energy, area minimal deflections were relaxed using the 2 dimensional model in question and Morpho. Both simulators were given representations of the same piecewise deflected disk and told to minimize area energy. This test allows comparison of how long both models take to return from far from equilibrium to equilibrium and the shapes they form.

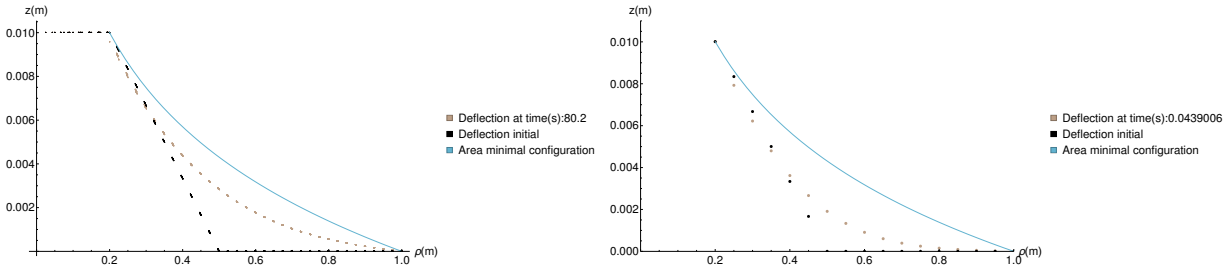

(a) Morpho

(b) 2D E-L gradient descent

Figure 4.3.1: Initially piecewise deflected liquid simulation frame 1

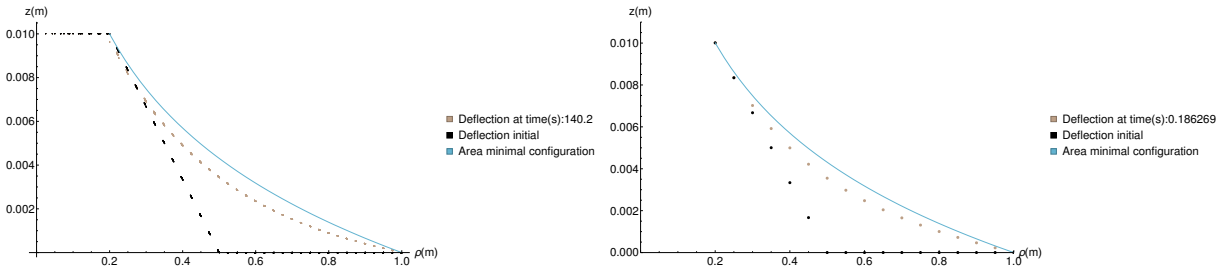

(a) Morpho (b) 2D E-L gradient descent

Figure 4.3.2: Initially piecewise deflected liquid simulation frame 2

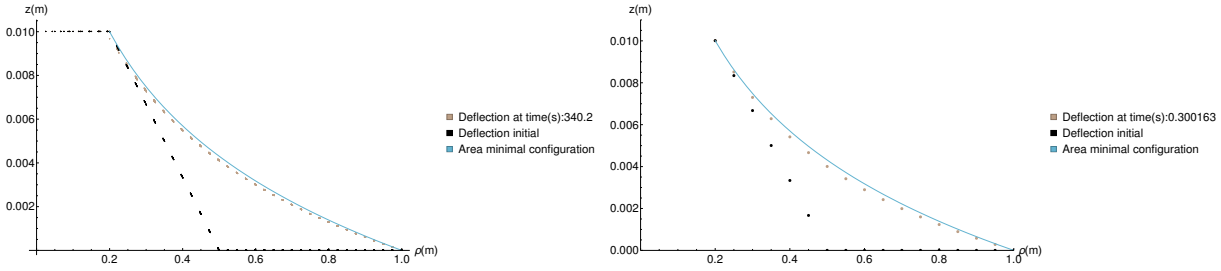

(a) Morpho (b) 2D E-L gradient descent

Figure 4.3.3: Initially piecewise deflected liquid simulation frame 3

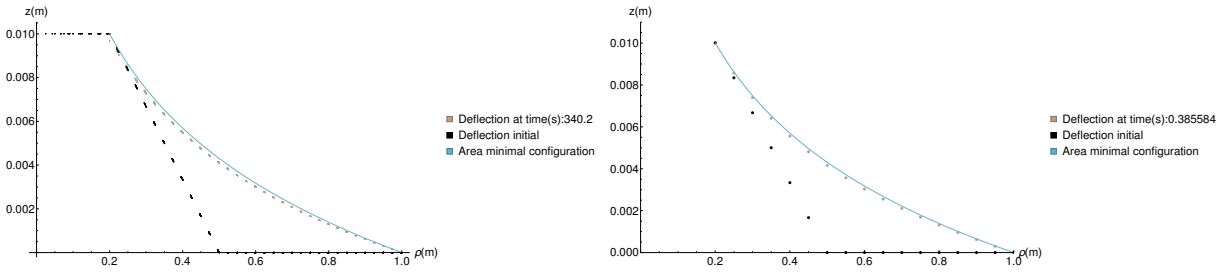

(a) Morpho (b) 2D E-L gradient descent

Figure 4.3.4: Initially piecewise deflected liquid simulation frame 4

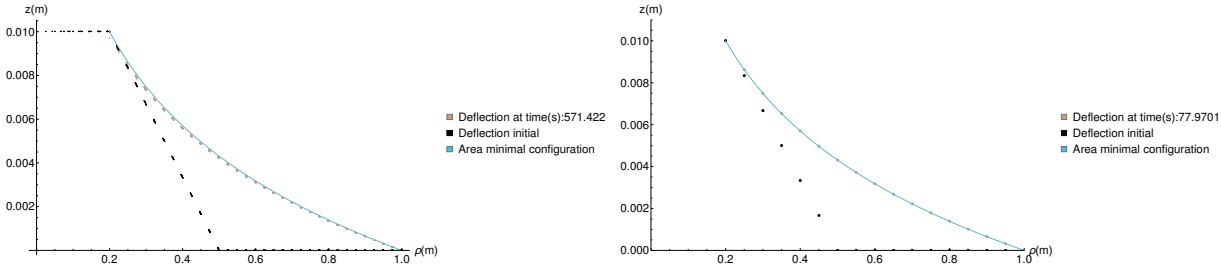

(a) Morpho (b) 2D E-L gradient descent

Figure 4.3.5: Initially piecewise deflected liquid simulation frame 5

The side by side comparison of the relaxation behavior of Morpho and Euler-Lagrange minimizer shows that the timescale of the Euler-Lagrange minimizer is more physically plausible than Morpho but that both follow a similar path to equilibrium. Morpho during these simulations, while theoretically modeling a suddenly deflected dish of water, claims the water will take many minutes in real time to reach equilibrium. On the other hand the Euler-Lagrange minimizer indicates that the dish should reach equilibrium in a fraction of

a second. However both take paths towards equilibrium which appear very similar.

Bibliography

[1] Lattice light-sheet microscopy: Imaging molecules to embryos at high spatiotemporal resolution | science.

[2] Martial Balland, Nicolas Desprat, Delphine Icard, Sophie Féréol, Atef Asnacios, Julien Browaeys, Sylvie Hénon, and François Gallet. Power laws in microrheology experiments on living cells: Comparative analysis and modeling. 74(2):021911.

[3] Eric Bertin, Michel Droz, and Guillaume Grégoire. Hydrodynamic equations for self-propelled particles: microscopic derivation and stability analysis. 42(44):445001.

[4] Edward Bormashenko. Progress in understanding wetting transitions on rough surfaces. 222:92–103.

[5] Edward Bormashenko. Young, boruvka-neumann, wenzel and cassie-baxter equations as the transversality conditions for the variational problem of wetting. 345.

[6] Edward Bormashenko, Gene Whyman, Yelena Bormashenko, Roman Grynyov, Evgeny Shulzinger, and Alexander Kazachkov. Sagging ropes demonstrate transversality conditions of variational problems. 83(12):998–1002.

[7] B.-C. Chen, W. R. Legant, K. Wang, L. Shao, D. E. Milkie, M. W. Davidson, C. Janetopoulos, X. S. Wu, J. A. Hammer, Z. Liu, B. P. English, Y. Mimori-Kiyosue, D. P. Romero, A. T. Ritter, J. Lippincott-Schwartz, L. Fritz-Laylin, R. D. Mullins, D. M. Mitchell, J. N. Bembenek, A.-C. Reymann, R. Bohme, S. W. Grill, J. T. Wang, G. Seydoux, U. S. Tulu, D. P. Kiehart, and E. Betzig. Lattice light-sheet microscopy: Imaging molecules to embryos at high spatiotemporal resolution. 346(6208):1257998–1257998.

[8] Stephen J. DeCamp, Gabriel S. Redner, Aparna Baskaran, Michael F. Hagan, and Zvonimir Dogic. Orientational order of motile defects in active nematics. 14(11):1110–1115.

[9] Masao Doi. *Soft Matter Physics*. Oxford University Press.

[10] Yaouen Fily, Aparna Baskaran, and Michael F. Hagan. Active particles on curved surfaces.

[11] Jun Geng, Jonathan V. Selinger, and Robin L. B. Selinger. Coarse-grained modeling of a deformable nematic vesicle. 9(34):8314.

[12] Hitoshi Gotoh, Akio Okayasu, and Yasunori Watanabe. *Computational Wave Dynamics*, volume 37 of *Advanced Series on Ocean Engineering*.

[13] Linda S. Hirst, Adam Ossowski, Matthew Fraser, Jun Geng, Jonathan V. Selinger, and Robin L. B. Selinger. Morphology transition in lipid vesicles due to in-plane order and topological defects. 110(9):3242–3247.

[14] Raouf A. Ibrahim. *Liquid Sloshing Dynamics: Theory and Applications*. Cambridge University Press.

[15] Katharine E. Jensen, Raphael Sarfati, Robert W. Style, Rostislav Boltyanskiy, Aditi Chakrabarti, Manoj K. Chaudhury, and Eric R. Dufresne. Wetting and phase separation in soft adhesion. 112(47):14490–14494.

[16] Jean-François Joanny and Sriram Ramaswamy. A drop of active matter. 705:46–57.

[17] Felix C. Keber, Etienne Loiseau, Tim Sanchez, Stephen J. DeCamp, Luca Giomi, Mark J. Bowick, M. Cristina Marchetti, Zvonimir Dogic, and Andreas R. Bausch. Topology and dynamics of active nematic vesicles. 345(6201):1135–1139.

[18] T. Lopez-Leon, V. Koning, K. B. S. Devaiah, V. Vitelli, and A. Fernandez-Nieves. Frustrated nematic order in spherical geometries. 7(5):391–394.

[19] M. C. Marchetti, J. F. Joanny, S. Ramaswamy, T. B. Liverpool, J. Prost, Madan Rao, and R. Aditi Simha. Hydrodynamics of soft active matter. 85(3):1143–1189.

[20] Andreas M. Menzel. Tuned, driven, and active soft matter. 554:1–45.

[21] Michael Mikucki and Y. C. Zhou. Fast algorithm for simulating lipid vesicle deformation i: Spherical harmonic approximation.

[22] Shradha Mishra, Aparna Baskaran, and M. Cristina Marchetti. Fluctuations and pattern formation in self-propelled particles. 81(6).

[23] Peter Müller and Hans Von Storch. *Computer Modelling in Atmospheric and Oceanic Sciences*. Springer.

[24] Thomas R. Powers, Greg Huber, and Raymond E. Goldstein. Fluid-membrane tethers: Minimal surfaces and elastic boundary layers. 65(4):041901.

[25] William Press, Saul Teukolsky, William Vetterling, and Brian Flannery. *Numerical Recipes*. Cambridge University Press, 32 Avenue of the Americas, New York, NY 10013-2473, USA, 2007.

[26] Elias Putzig, Gabriel S. Redner, Arvind Baskaran, and Aparna Baskaran. Instabilities, defects, and defect ordering in an overdamped active nematic.

[27] Rastko Sknepnek and Silke Henkes. Active swarms on a sphere. 91(2):022306.

[28] Rafael Tadmor. Line energy and the relation between advancing, receding, and young contact angles. 20(18):7659–7664.

[29] E. M. Terentjev and David A. Weitz, editors. *The Oxford handbook of soft condensed matter*. Oxford handbooks. Oxford University Press.

[30] Sumesh P. Thampi, Amin Doostmohammadi, Ramin Golestanian, and Julia M. Yeomans. Intrinsic free energy in active nematics. *EPL (Europhysics Letters)*, 112(2):28004, 2015.

[31] John Toner and Yuhai Tu. Long-range order in a two-dimensional dynamical **XY** model: How birds fly together. 75(23):4326–4329.

[32] Matthew A. Glaser M.D. Betterton Tong Gao, Robert Blackwell and Michael J. Shelley. Multiscale polar theory of microtubule and motor-protein assemblies. 114(4).

[33] Tams Vicsek, Andrs Czirk, Eshel Ben-Jacob, Inon Cohen, and Ofer Shochet. Novel type of phase transition in a system of self-driven particles. 75(6):1226–1229.

[34] Yunjie Wang, Shahrokh Zeinali-Davarani, Elaine C. Davis, and Yanhang Zhang. Effect of glucose on the biomechanical function of arterial elastin. 49:244–254.

[35] Hongyan Yuan, Changjin Huang, Ju Li, George Lykotrafitis, and Sulin Zhang. One-particle-thick, solvent-free, coarse-grained model for biological and biomimetic fluid membranes. 82(1):011905.